Publications of the Astronomical Society of the Pacific, **122**:261–287, 2010 March

The Herschel Reference Survey

A. Boselli,[1] S. Eales,[2] L. Cortese,[2] G. Bendo,[3] P. Chanial,[3] V. Buat,[1] J. Davies,[2] R. Auld,[2] E. Rigby,[4] M. Baes,[5] M. Barlow,[6] J. Bock,[7] M. Bradford,[7] N. Castro-Rodriguez,[8] S. Charlot,[9] D. Clements,[3] D. Cormier,[10] E. Dwek,[11] D. Elbaz,[10] M. Galametz,[10] F. Galliano,[12] W. Gear,[2] J. Glenn,[13] H. Gomez,[2] M. Griffin,[2] S. Hony,[10] K. Isaak,[2] L. Levenson,[7] N. Lu,[7] S. Madden,[10] B. O'Halloran,[3] K. Okamura,[10] S. Oliver,[14] M. Page,[15] P. Panuzzo,[10] A. Papageorgiou,[2] T. Parkin,[16] I. Perez-Fournon,[8] M. Pohlen,[2] N. Rangwala,[13] H. Roussel,[9] A. Rykala,[2] N. Sacchi,[17] M. Sauvage,[10] B. Schulz,[18] M. Schirm,[16] M. W. L. Smith,[2] L. Spinoglio,[17] J. Stevens,[19] M. Symeonidis,[19] M. Vaccari,[20] L. Vigroux,[9] C. Wilson,[16] H. Wozniak,[21] G. Wright,[19] and W. Zeilinger[22]

Received 2008 August 17; accepted 2010 January 26; published 2010 February 26

ABSTRACT. The Herschel Reference Survey is a Herschel guaranteed time key project and will be a benchmark study of dust in the nearby universe. The survey will complement a number of other Herschel key projects including large cosmological surveys that trace dust in the distant universe. We will use Herschel to produce images of a statistically-complete sample of 323 galaxies at 250, 350, and 500 μm. The sample is volume-limited, containing sources with distances between 15 and 25 Mpc and flux limits in the K band to minimize the selection effects associated with dust and with young high-mass stars and to introduce a selection in stellar mass. The sample spans the whole range of morphological types (ellipticals to late-type spirals) and environments (from the field to the center of the Virgo Cluster) and as such will be useful for other purposes than our own. We plan to use the survey to investigate (i) the dust content of galaxies as a function of Hubble type, stellar mass, and environment; (ii) the connection between the dust content and composition and the other phases of the interstellar medium; and (iii) the origin and evolution of dust in galaxies. In this article, we describe the goals of the survey, the details of the sample and some of the auxiliary observing programs that we have started to collect complementary data. We also use the available multifrequency data to carry out an analysis of the statistical properties of the sample.

Online material: color figures

1. INTRODUCTION

Understanding the processes that govern the formation and evolution of galaxies is one of the major challenges of modern astronomy. Ideally this work can be done by analyzing and comparing the physical, structural and kinematical properties of different objects at various epochs to model predictions. How primordial galaxies transform their huge gas reservoir into stars

[1] Laboratoire d'Astrophysique de Marseille, UMR6110 CNRS, 38 rue F. Joliot-Curie, F-13388 Marseille, France.

[2] School of Physics and Astronomy, Cardiff University, Queens Buildings The Parade, Cardiff CF24 3AA, UK.

[3] Astrophysics Group, Imperial College, Blackett Laboratory, Prince Consort Road, London SW7 2AZ, UK.

[4] School of Physics & Astronomy, University of Nottingham, University Park, Nottingham NG7 2RD, UK.

[5] Sterrenkundig Observatorium, Universiteit Gent, Krijgslaan 281 S9, B-9000 Gent, Belgium.

[6] Department of Physics and Astronomy, University College London, Gower Street, London WC1E 6BT, UK.

[7] Jet Propulsion Laboratory, Pasadena, CA 91109, Department of Astronomy, California Institute of Technology, Pasadena, CA 91125.

[8] Instituto de Astrofísica de Canarias, C/Va Lctea s/n, E-38200 La Laguna, Spain.

[9] Institut d'Astrophysique de Paris, UMR7095 CNRS, Université Pierre & Marie Curie, 98 bis Boulevard Arago, F-75014 Paris, France.

[10] Laboratoire AIM, CEA/DSM–CNRS–Université Paris Diderot, Irfu/Service d'Astrophysique, 91191 Gif sur Yvette, France.

[11] Observational Cosmology Lab, NASA Goddard Space Flight Center, Greenbelt, MD 20771.

[12] Department of Astronomy, University of Maryland, College Park, MD 20742.

[13] Department of Astrophysical and Planetary Sciences, University of Colorado, Boulder, CO 80309.

[14] Astronomy Centre, Department of Physics and Astronomy, University of Sussex, UK.

[15] Mullard Space Science Laboratory, University College London, Holmbury St Mary, Dorking, Surrey RH5 6NT, UK.

[16] Dept. of Physics & Astronomy, McMaster University, Hamilton, Ontario L8S 4M1, Canada.

[17] Istituto di Fisica dello Spazio Interplanetario, INAF, Via del Fosso del Cavaliere 100, I-00133 Rome, Italy.

[18] Infrared Processing and Analysis Center, California Institute of Technology, Pasadena, CA 91125.

and become the objects that we now observe in the local universe is a key question. A wide coverage of the electromagnetic spectrum to probe the atomic (21 cm line) and molecular (generally through the 2.6 mm CO line) gas components, the different stellar populations (UV to near-IR spectral range), the dust (mid- and far-IR) and the electrons in magnetic fields (radio continuum) is necessary to address this important question.

The importance of dust resides in the fact that it is formed from the aggregation of the metals produced in the latest phases of stellar evolution, and contains approximately half the metals in the interstellar medium (Whittet 1992). Injected into the interstellar medium (ISM) by stellar winds and supernovae explosions, dust acts as a catalyst in the process of transformation of the atomic to molecular hydrogen necessary to feed star formation (Hollenbach & Salpeter 1971; Duley & Williams 1986). Dust also contributes to the shielding of the UV radiation field, preventing the dissociation of molecular clouds, and thus playing a major role in the energetic equilibrium of the ISM (Hollenbach & Tielens 1997). Dust contributes to the cooling and heating of the ISM in photodissociation regions through photoelectric heating. Furthermore, by absorbing the stellar light, dust modifies our view of the different stellar components (e.g., Buat & Xu 1996): because dust obscuration is so important in star-forming regions, the emission from dust is one of the most powerful tracers of the star formation activity in galaxies (Kennicutt 1998; Hirashita et al. 2003). Dust emission can therefore be used to study the relationship between the gas surface density and the star formation activity, generally known as the Schmidt law.

The importance of dust in the study of the formation and evolution of galaxies became evident after the IRAS space mission which provided us with a whole sky coverage in four infrared bands. Despite its low sensitivity and poor angular resolution, IRAS detected tens thousands of extragalactic sources (Soifer et al. 1987). The IRAS survey showed that the stellar light in some galaxies is so heavily obscured that the only way to determine their star formation activity is through the dust emission itself. Among these highly obscured galaxies, the Ultraluminous Infrared Galaxies (ULIRGs) are the most actively star-forming objects in the local universe. With their improved sensitivity, spectral and angular resolution, other space missions such as ISO and *Spitzer* have brought a better understanding of the chemical and physical properties of interstellar dust in a wide range of different galactic and extragalactic sources. IRAS, ISO, *Spitzer*, and the recently launched AKARI satellite, however, are sensitive to dust emitting in the mid- (~$5\ \mu$m) to far- (≤$200\ \mu$m) infrared domain. The 5–70 μm spectral range corresponds to the emission of the hot dust generally associated to star formation, while at longer wavelengths, up to 1 mm, the contribution of cold dust becomes more and more important (Draine et al. 2007). The emission of the ISM in the range $3\ \mu\mathrm{m} \lesssim \lambda \lesssim 15\ \mu\mathrm{m}$ is generally dominated by polycyclic aromatic hydrocarbons (PAHs). Between 10 μm and $\lesssim 70\ \mu$m the dust emission is usually due to very small grains, while that at longer wavelengths ($70\ \mu\mathrm{m} \lesssim \lambda \lesssim 1000\ \mu\mathrm{m}$) is probably produced by large grains of graphite and silicate in thermal equilibrium with the UV and optical photons of the interstellar radiation field (Désert et al. 1990; Dwek et al. 1997; Zubko et al. 2004; Draine & Li 2007).

There is, however, strong empirical evidence to suggest that much of the dust in normal galaxies has been missed by previous space missions because it is too cold to radiate in the mid- and far-infrared. Devereux & Young (1990), for example, showed that when the dust masses of galaxies were estimated from IRAS data, the gas-to-dust ratios were $\simeq 10$ times higher than the Galactic value, implying that 90% of the dust in galaxies is too cold to radiate significantly in the IRAS bands. ISO 200 μm images of nearby galaxies revealed the presence of cold (~20 K) dust in the external parts of galaxies (Alton et al. 1998). Even *Spitzer*, with its longer wavelength coverage, is only sensitive to dust that is warmer than $\simeq 15$ K (Bendo et al. 2003; Draine & Li 2007; Draine et al. 2007). Simple estimates show that the temperature of a dust grain in thermal equilibrium in the average interstellar radiation field is ~20 K, which would produce a modified black body spectrum with a peak at ~$200\ \mu$m with a flux rapidly decreasing at longer wavelengths (Boselli et al. 2003a; Dale et al. 2005, 2007; Draine & Li 2007; Draine et al. 2007). It is important to remember, however, that most of the dust in a galaxy is likely to be at a much lower temperature than 20 K because it is self-shielded, and so unaffected from the interstellar radiation field. For example, in molecular clouds the temperature of the dust is usually well below the canonical 20 K value once the average dust extinction (A_V) is greater than one, unless it is close to a newly formed star (Ward-Thompson et al. 2002).

The submillimeter waveband (200–1000 μm) is crucial for detecting this missing cold dust component and thus for making accurate estimates of the total dust mass. Mass estimates made from far-infrared measurements are highly uncertain because of the strong dependence of flux on dust temperature which is difficult to determine using data on the Wien side of the black body peak. At long wavelengths (Rayleigh-Jeans domain) the emissivity depends only on the first power of the dust temperature, making it possible to use a submillimeter flux to make an accurate estimate of the mass of dust (Eales et al. 1989; Galliano et al. 2003; 2005).

Submillimeter continuum observations of galaxies have been made previously, in particular with the ground-based submillimeter cameras, such as SCUBA on the James Clerk Maxwell

[19] Centre for Astrophysics Research, Science and Technology Research Centre, University of Hertfordshire, College Lane, Herts AL10 9AB, UK.

[20] University of Padova, Department of Astronomy, Vicolo Osservatorio 3, I-35122 Padova, Italy.

[21] Observatoire Astronomique de Strasbourg, UMR 7550 Université de Strasbourg–CNRS, 11, rue de l'Université, F-67000 Strasbourg, France.

[22] Institut für Astronomie, Universität Wien, Türkenschanzstr. 17, A-1180 Wien, Austria.

Telescope. These have confirmed that galaxies do indeed contain a large amount of cold dust (Dunne & Eales 2001; Galliano et al. 2003). Until now, the largest submillimeter survey has been the SCUBA Local Universe and Galaxy Survey (SLUGS), a survey of $\simeq$200 galaxies in two samples, one selected from the IRAS survey and one selected at optical wavelengths. The survey produced the first estimates of the submillimeter luminosity and dust-mass (the space density of galaxies as a function of dust mass) functions (Dunne et al. 2000; Vlahakis et al. 2005), and also indicated that some ellipticals are surprisingly strong submillimeter sources. Its limitation, and the limitation of all ground-based submillimeter observations, is that of sensitivity: SLUGS struggled to detect galaxies not already detected by IRAS.

The solution is to go into space and the Herschel space telescope is finally making this possible. In particular the relatively large field of view, high sensitivity, and coverage of a waveband (250–500 μm) in which galaxies are intrinsically bright, make SPIRE on Herschel the ideal instrument for a study of all extragalactic sources (Griffin et al. 2006, 2007; Wasket et al. 2007). SPIRE has the sensitivity to map large areas of the sky down to the confusion limit in quite modest integration times, providing submillimeter data for large samples of galaxies at different redshifts, and is thus well adapted for pointed observations for all kind of nearby extragalactic sources.

The SPIRE consortium has defined a number of coordinated guaranteed time programs to get the best possible benefit of the unique Herschel facilities for the study of galaxy evolution. These include deep cosmological surveys, pointed observations of local galaxies and surveys of representative regions in the Milky Way. To better characterize the dust properties in the local universe, the SPIRE extragalactic group has selected a volume-limited sample of 323 galaxies to be observed in guaranteed time in the three SPIRE bands at 250, 350, and 500 μm. The importance of the local universe resides in the fact that it represents the endpoint of galaxy evolution, providing important boundary conditions to models and simulations. Furthermore, at $\leq$30 Mpc the angular resolution of SPIRE (a couple of kpc) allow us to resolve the different galaxy components such as nuclei, bulges, disks, and spiral arms. Moreover, dwarf galaxies, by far the most common (yet still very poorly understood) galaxies in the universe, can only be observed locally.

A volume-limited sample was chosen as a way to limit distance dependent selection biases. To limit any possible contamination due to the cosmic variance, the volume should be much larger than the typical dimension of large-scale structures (~30 Mpc). At the same time it should be representative of the whole galaxy population inhabiting the local universe. A near-infrared K-band selection was adopted for two major reasons: (i) unlike optical surveys, which have strong selection effects due to the presence of dust, near-IR data are only marginally affected by dust extinction; (ii) whereas the optical flux is highly dependent on the number of relatively young stars and thus sensitive to recent episodes of star formation, the near-IR luminosity is a good measure of the overall stellar mass (e.g., Gavazzi et al. 1996), which recent studies suggest as the most important parameter in characterizing the statistical and evolutionary properties of galaxies. Indeed galaxy properties that appear to be tightly correlated with the galaxy's stellar mass include the following: physical properties, such as the star formation activity, the gas content and the metallicity (Boselli et al. 2001; 2002a; Zaritsky et al. 1994; Gavazzi et al. 2004; Tremonti et al. 2004); structural properties, such as the concentration index and the galaxy's light profile (Boselli et al. 1997; Gavazzi et al. 2000a; Scodeggio et al. 2002); the amount and distribution of dark matter, as indicated by the Tully-Fisher relation and the shape of the rotation curve for spirals (Tully & Fisher 1977; Catinella et al. 2006) and the fundamental plane for ellipticals (Dressler et al. 1987; Djorgovski & Davis 1987); the stellar population, shown through the color-magnitude relations for early-type (Visvanathan & Sandage 1977, Bower et al. 1992) and late-type galaxies (Tully et al. 1982, Gavazzi et al. 1996) and the galaxy spectral energy distributions (Gavazzi et al. 2002b, Kauffmann et al. 2003). These correlations all indicate a down-sizing effect (e.g., Gavazzi et al. 1996; Cowie et al. 1996; Heavens et al. 2004), in which galaxies with high stellar masses formed most of their stars at a much earlier cosmic epoch than those with low stellar masses. This underline the dominant role of mass, rather than morphology, in shaping galaxies.

The final sample includes galaxies with a large range in luminosity (mass) and includes all Hubble types. Because of its definition, the selected sample also includes galaxies belonging to different density regions such as the core of the Virgo cluster, groups and pairs and isolated objects. Given its completeness, the Herschel Reference Sample (HRS) will be a suitable reference for any statistical study. Combined with KINGFISH (the Herschel extension of SINGS, Kennicutt et al. 2003) and VNGS (see § 3, footnote 23), two samples optimized for the study of the different phases of the ISM in individual galaxies, these samples will provide the community with a unique dataset for studying the ISM properties of galaxies in the local universe.

The paper is organized as follows. Section 2 describes the scientific goals of the survey. Section 3 gives a description of the selection criteria used to define the sample. Section 4 gives details of the SPIRE observations we will carry out and § 5 gives an overview of the multifrequency data that is available for the sample. Section 6 gives a brief description of the data processing and products. The multifrequency statistical properties of the sample will be described in § 7.

2. SCIENTIFIC OBJECTIVES

The overall goal of this Herschel survey is to improve our knowledge of the cold dust properties of the most common extragalactic sources populating the local universe. Combined with multifrequency ancillary data covering the entire electromagnetic spectrum (see § 5), the new Herschel data will provide us with a unique data set with which to:

1. Trace, for the first time, the variation of the properties of the cold dust component (dust mass and temperature, dust to gas ratio,z…) of normal galaxies along the Hubble sequence, and as a function of luminosity. Given the large dispersion in galaxy properties (Morton & Haynes 1994), it is important that the sample to be large enough to contain representatives of all galaxy types and include both early- and late-type galaxies spanning the largest possible range in luminosity. Where galaxies are resolved, we can analyze the distribution of the cold dust in the different galaxy components, e.g., the nuclei, bulges, spiral arms, and diffuse disks. This will provide important constraints on dust formation and evolution in galaxies (Galliano et al. 2008).

2. Study the role of dust in the physics of the ISM. As discussed in the introduction, dust plays a major role in the energetic equilibrium of the ISM. It acts as catalyst for the formation of the molecular hydrogen (Hollenbach & Salpeter 1971; Duley & Williams 1986) and shields the molecular gas component preventing dissociation from the diffuse interstellar radiation field (Hollenbach & Tielens 1997). To understand the nature of the ISM we thus need to know how the cold dust properties (temperature, composition, geometrical distribution…) relate to other physical properties such as metallicity and interstellar radiation field (Boselli et al. 2004; Galliano et al. 2008). By combining dust surface brightnesses with metallicity dependent gas-to-dust ratios and HI column densities, submillimeter measurements can be used to determine H_2 column densities (Guélin et al. 1993; 1995; Neininger et al. 1996; Boselli et al. 2002a). SPIRE data will therefore provide us with an independent measure of the molecular hydrogen component, and can be use for an accurate calibration of the still highly uncertain CO to H_2 conversion factor.

3. Study the relationship between dust emission and star formation. Dust participates in the cooling of the gas through the shielding of the interstellar radiation field, in particular of the UV light, and thus plays a major role in the process of star formation (Draine 1978; Dwek 1986; Hollenbach & Tielens 1997). The energy absorbed by dust is then radiated in the infrared domain. For the same reason dust emission has often been used as a tracer of star formation. We still do not know, however, what is the relationship between the cold dust emission and star formation. The study of resolved galaxies will allow us to analyze the relationship between the infrared surface brightness and the dust temperature (Chanial et al. 2007) and to trace the connections between the star formation and the dust and gas properties at galactic scales, extending the recent results of *Spitzer* to all phases of the ISM (Gordon et al. 2004, Calzetti et al. 2005, 2007; Perez-Gonzalez et al. 2006; Kennicutt et al. 2007, Prescott et al. 2007; Thilker et al. 2007).

4. Study the dust extinction properties in galaxies. Astronomers have tackled with the problem of dust opacity in galaxies for over 40 yr (e.g., Holmberg 1958; Disney et al. 1989; Calzetti 2001), but have reached no consensus. The key problem is that optical catalogs contain huge selection effects because of the existence of dust. We will be able to address this issue in two ways. First, the submillimeter images will, for the first time, allow us to determine the distribution of the dust column density in a very large number of galaxies. Second, we will be able to determine the global dust opacity in each galaxy by using the energy balance between the absorbed stellar light and the dust emitted radiation (Buat & Xu 1996, Witt & Gordon 2000, Buat et al. 2002, Cortese et al. 2006; 2008a). This requires an accurate determination of the UV to near-IR (stellar light) and mid-IR to submillimeter (dust emission) spectral energy distribution (Boselli et al. 2003a). By comparing the dust attenuation properties of different classes of objects, this analysis will allow us to define standard recipes for correcting UV and optical data, a useful tool for the interpretation of all modern surveys.

5. Determine whether there is an intergalactic dust cycle. Apart from the obvious possibility that dust is ejected from galaxies by the same methods that gas is ejected, such as through interactions with the surrounding environment (see point 9) and starburst-driven "superwinds" as indeed observed in M82 (Engelbracht et al. 2006), there is also the possibility that dust is ejected from galaxies by radiation pressure (Davies et al. 1998, Meiksin 2009, Oppenheimer & Davé 2008). The ejection of dust from galaxies might explain the huge reservoir of metals found in the intergalactic medium (Rayan-Weber et al. 2006). There is clear evidence for dust in superwinds (Alton et al. 1999) and there is tantalizing evidence from ISO observations for extended distributions of dust around galaxies (Alton et al. 1998; Davies et al. 1999). Observations so far have been limited by either sensitivity (SCUBA) or resolution (ISO and Spitzer). The Herschel Reference Survey will be able to determine whether dust ejection is important because (i) we will be observing several hundred galaxies, so even if these phenomena are rare our sample should contain some examples, and (ii) our observations will have the sensitivity to detect dust well outside the optical disk of each galaxy.

6. Determine the amount of interstellar dust in ellipticals. Very little is known about dust in ellipticals. Despite the stereotype that ellipticals do not contain any dust, the structures seen in optical images imply that at least 50% of ellipticals contain some dust (Ferrarese et al. 2006). The amount of interstellar dust is too small, however, to be easily detected through its far-infrared emission; IRAS, for example, detected only about 15% of ellipticals (Bregman et al. 1998). Although Spitzer has now detected many ellipticals, these studies have mostly been of sources known a priori to contain some dust (Kaneda et al. 2007; Temi et al. 2007; Panuzzo et al. 2007) or molecular gas (Young et al. 2008). The SLUGS did contain a small statistically-complete sample of 11 ellipticals, although some of the six 850 μm detections may well have been of synchrotron rather than dust emission (Vlahakis et al. 2005). Other ellipticals

have been detected at 350 μm by Leeuw et al. (2008). The HRS contains 65 early-type (E, S0, and S0a) galaxies and our observations will have sufficient sensitivity to detect dust masses down to ~$10^4\ M_\odot$. The Herschel Reference Survey will therefore provide an unambiguous answer to the question of how much dust is in ellipticals.

7. Determine the origin of dust in ellipticals. The three possible origins of the dust in ellipticals are that (i) it has been produced in the atmospheres of the old evolved stars that dominate the light of ellipticals today, (ii) its origin is external to the elliptical and is the result of a merger, (iii) it is the relic of dust formed during the active star-forming phase early in the history of the galaxy. The distribution of dust is an important clue to understand its true origin. The presence of the first mechanism is suggested by Spitzer mid-infrared spectra of Virgo ellipticals (Bressan et al. 2006) which show the silicate emission produced by dust in circumstellar envelopes of evolved stars. The origin of this feature (predicted by Bressan et al. 1998) is supported by the finding that the mid-infrared emission has the same profile as optical light (Xilouris et al. 2004) in many early-type galaxies. It is unclear, however, whether this is the predominant mechanism producing the interstellar dust in these galaxies. For example, a submillimeter map of the nearby elliptical Centaurus A, has revealed a dusty disk, implying that the dust (and the galaxy itself) has been formed as the result of a merger (Leeuw et al. 2002). Temi et al. (2007) also found little correlation between the Spitzer 70 and 160 μm emission and optical starlight, which also suggests the dust has an external origin.

We will use the Herschel Reference Survey results to investigate the origin of the dust by, first, investigating the detailed morphology of the dust, in particular how it compares with the stellar distribution, and, second, by investigating whether the mass of dust is correlated with other global properties of the galaxy such as stellar mass. It has often been argued that sputtering by the ubiquitous, hot X-ray emitting gas in early galaxies should destroy any dust formed more than 10^8 years in the past (Tielens et al. 1994). However, the fact that dust is seen visually in 50% of ellipticals (Ferrarese et al. 2006) and the recent discovery of small grains, which are preferentially destroyed by sputtering, in ellipticals (Kaneda et al. 2007) suggests that dust is protected in some way. We will investigate whether sputtering from the hot gas destroys the dust grains and will test the internal origin hypothesis by investigating any possible correlation between X-ray excess and dust mass.

8. Measure the local luminosity and dust-mass distributions. These distributions are important benchmarks for the deep Herschel surveys. These have already been estimated as part of SLUGS (Dunne et al. 2000; Vlahakis et al. 2005): the much greater sensitivity of the Herschel Reference Survey will push these limits down by a factor of ~50.

9. Understand the role of the environment on the evolution of galaxies. The well-known phenomenon that spiral galaxies in clusters are HI-deficient and have truncated HI disks (e.g., Cayatte et al. 1990) demonstrates that the environment of a galaxy can have a strong effect on its interstellar medium. Indeed there is clear evidence for tidally-stripped dust in interacting galaxies (Thomas et al. 2002) and indications for ram-pressure stripped dust in cluster objects (Boselli & Gavazzi 2006). At the same time the presence of metals (Sarazin 1986) and possibly of dust (Stickel et al. 2002; Montier & Giard 2005) in the diffuse intracluster medium has been shown by X-ray and far-IR observations. The comparison of the submillimeter emission of cluster and isolated galaxies within the HRS will allow us to make a detailed study on the effects of the environment on the dust properties of galaxies, and thus understand whether the hot and dense cluster intergalactic medium can be polluted through the gas stripping process of late-type galaxies (Boselli & Gavazzi 2006).

10. Provide a multifrequency reference sample suitable for any statistical study. Our aim is that the HRS will be the first large sample of galaxies with observations of all phases of the ISM, as well as measurements over the entire wavelength range of the spectral energy distribution (SED) for each galaxy. The sample will then serve for many purposes; e.g., the UV to radio continuum SEDs could, for example, be used to determine the nature of unresolved sources or as templates for estimating photometric redshifts.

3. THE SAMPLE

The Herschel Reference Sample (HRS) has been selected according to the following criteria:

1. Volume-limited: A volume limit was imposed to reduce distance uncertainties due to local peculiar motions and ensure the presence of low-luminosity, dwarf galaxies, not accessible at high redshift. By applying a lower distance (D) limit we exclude the very extended sources, the observing of which would be too time consuming[23]. We have selected all galaxies with an optical recessional velocity (vel, taken from NED) in between $1050\ \mathrm{km\,s^{-1}}$ and $1750\ \mathrm{km\,s^{-1}}$ that, for $\mathrm{H_0} = 70\ \mathrm{km\,s^{-1}}$ $\mathrm{Mpc^{-1}}$ and in the absence of peculiar motions, corresponds to $15 \leq D \leq 25$ Mpc[24]. In the Virgo cluster region ($12^\mathrm{h} <$ R.A.$(2000) < 13^\mathrm{h}$; $0° <$ decl. $< 18°$), where peculiar motions are dominant, we have included all galaxies with vel $<$ $3000\ \mathrm{km\,s^{-1}}$ and belonging to cluster A, the North (N) and East (E) clouds, and the Southern extension (S) (17 Mpc) and Virgo B (23 Mpc), where the subgroup membership has been taken from Gavazzi et al. (1999a). W and M clouds objects, at a distance of 32 Mpc, have been excluded.[25]

[23] A small sample of very nearby and extended galaxies will be observed in detail as part of another guaranteed time project: Physical Processes in the Interstellar Medium of Very Nearby Galaxies.

[24] Given the possible discrepancy between optical and HI recessional velocity measurements, heliocentric velocities given in Table 1 can be outside this range.

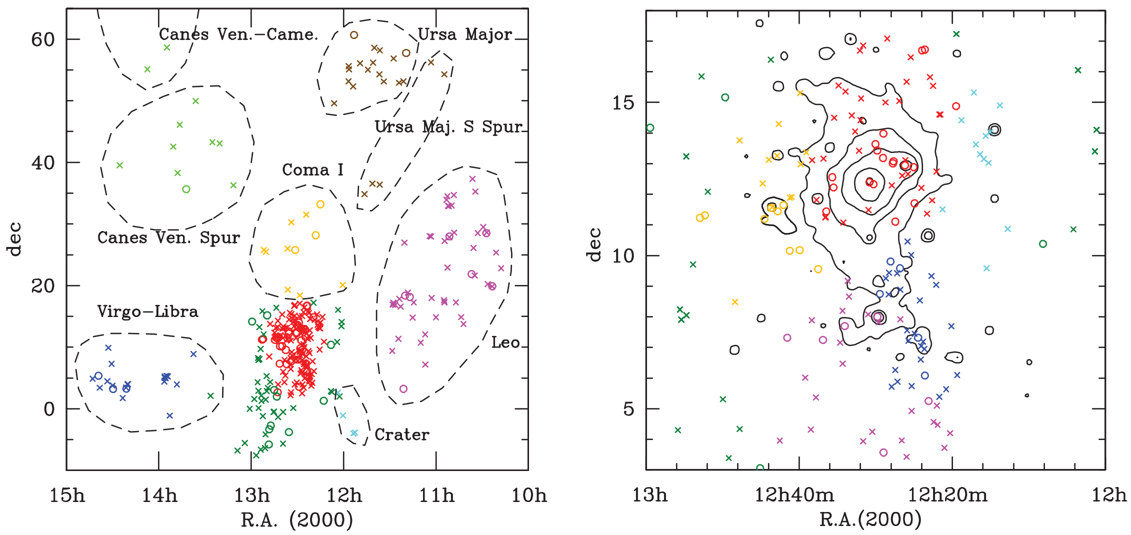

FIG. 1.—Sky distribution of the HRS for early-type (E-S0-S0a; *circles*) and late-type (Sa-Sd-Im-BCD; *crosses*) galaxies (*left panel*). *Dashed contours* delimit the different clouds. The large concentration of galaxies in the center of the figure is the Virgo cluster (*red*) with its outskirts (*dark green*) *Orange symbols* are for Coma I Cloud, *magenta* for Leo Cloud, *brown* for Ursa Major Southern Spur and Cloud, *cyan* for Crater Cloud, *light green* for Canes Venatici Spur and Camelopardalis, and *blue* for Virgo-Lybra Cloud galaxies, respectively. The Virgo cluster region (*right panel*): *black contours* show the diffuse X-ray emission of the cluster (from Böhringer et al. 1994). *Red symbols* are for galaxies belonging to the Virgo A cloud, *blue* to Virgo B, *orange* to Virgo E, *magenta* to Virgo S, *cyan* to Virgo N, and *dark green* to the Virgo outskirts, as defined by Gavazzi et al. (1999a).

2. K band selection: Given the expected low dust content of quiescent galaxies, whose emission would be hardly detectable within reasonable integration times, a more stringent limit has been adopted for early-types than for star-forming galaxies. Among those galaxies in the required recessional velocity range, we thus selected all late-type spirals and irregulars (Sa-Sd-Im-BCD) with a 2MASS K band total magnitude $K_{\mathrm{Stot}} \leq 12$ and all ellipticals and lenticulars (E, S0, S0a) with $K_{\mathrm{Stot}} \leq 8.7$.

3. High galactic latitude: To minimize galactic cirrus contamination, galaxies have been selected at high galactic latitude ($b > +55°$) and in low galactic extinction regions ($A_B < 0.2$; Schlegel et al. 1998).

The resulting sample is composed of 323 galaxies located in the sky region between $10^{\mathrm{h}}17^{\mathrm{m}} < \mathrm{R.A.}(2000) < 14^{\mathrm{h}}43^{\mathrm{m}}$ and $-6° < \mathrm{decl.} < 60°$ (see Fig. 1), of which 65 are early-type (E, S0 and S0a) and 258 are late-type (Sa-Sd-Im-BCD) (see Fig. 2). Figure 2 shows that the only galaxies which are clearly undersampled are blue compact galaxies and dwarf irregulars, the most numerous galaxies in the nearby universe. They will be the targets of another SPIRE key program.[26] As selected, the sample spans a large range in environment since it includes the Virgo cluster, many galaxy groups and pairs as well as relatively isolated objects (Fig. 1). Using the Virgo cluster membership criteria defined in Gavazzi et al. (1999a), the HRS includes 82 members of cluster A and B (Fig. 2) The other galaxies are members of nearby clouds such as Leo, Ursa Major and Ursa Major Southern Spur, Crater, Coma I, Canes Venatici Spur and Canes Venatici–Camelopardalis and Virgo-Libra Clouds (Tully 1988). As defined, the sample is thus ideal for environmental studies (Cortese & Hughes 2009; Hughes & Cortese 2009). The whole sample is given in Table 1 with columns arranged as follows:

Column 1: Herschel Reference Sample (HRS) name. This is the position of the galaxy in the sample list when sorted by increasing right ascension.

Column 2: Zwicky name, from the Catalogue of Galaxies and of Cluster of Galaxies (CGCG; Zwicky et al. 1961–1968).

Column 3: Virgo Cluster Catalogue (VCC) name, from Binggeli et al. (1985).

Column 4: Uppsala General Catalog (UGC) name (Nilson 1973).

Column 5: New General Catalogue (NGC) name.

Column 6: Index Catalogue (IC) name.

Column 7: J2000 right ascension, taken from NED.

Column 8: J2000 declinations, taken from NED.

Column 9: Morphological type, taken from NED, or from

[25] The sample was selected before distances were available on NED. According to these new NED estimates, the distance of the HRS galaxies outside the Virgo cluster are generally included in the $15 \leq D \leq 25$ Mpc range. In the Virgo region, however, our distances are determined according to subgroup membership criteria, and are thus generally different than those given by NED.

[26] The ISM in Low-Metallicity Environments: Bridging the Gap Between Local Universe and Primordial Galaxies

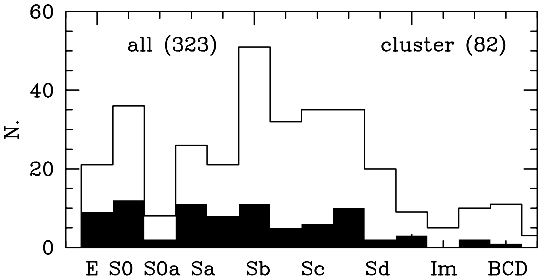

FIG. 2.—Distribution in morphological type of the HRS for all (*empty histogram*) and cluster (*filled histogram*) galaxies. The cluster sample is composed of galaxies members of the Virgo A and B clouds.

our own classification if not available.

Column 10: Total K band magnitude ($K_{\rm Stot}$), from 2MASS (Skrutskie et al. 2006).

Column 11: Optical isophotal distance D 25 (25 mag arcsec^{-2}), from NED.

Column 12: Heliocentric radial velocity (in km s^{-1}), from HI data when available, otherwise from NED.

Column 13: Cluster or cloud membership, from Gavazzi et al. (1999a) for Virgo, and Tully (1988) or Nolthenius (1993) whenever available, or from our own estimate otherwise.

Column 14: Pair/group membership, from Karachentsev et al. (1972) or from NED whenever available, or from our own estimate elsewhere. Pair/group membership has been assigned according to the following criteria: close pairs (CP) are those with a nearby companion at a distance less than 50 kpc and a difference in redshift $<$600 km s^{-1}, as in Gavazzi et al. (1999b), while pairs (P) up to 150 kpc. The number indicates whether the galaxy belongs to a triplet (3), quadruplet (4), and quintuplet (5). Groups outside Virgo and its immediate surroundings have been determined by counting the number of bright galaxies[27] within 25′ (which, at a median distance of 20 Mpc, corresponds to ∼150 kpc) and 600 km s^{-1}. Pairs in the Virgo region are only those catalogued by Karachentsev et al. (1972).

Column 15: Galactic extinction A_B (Schlegel et al. 1998).

Column 16: Alternative names.

4. SPIRE OBSERVATIONS

With its large field of view ($4' \times 8'$), its sensitivity ($S \sim 7$ mJy, 5σ in 1 hr, point source mode), and angular resolution (∼30 arcsec; see Table 2), SPIRE on Herschel is the ideal instrument for the proposed survey.

In constructing our observing program, we have used different integration times for early- and late-type galaxies because the former are known to contain less dust.

Integration times for early-types were determined by assuming a lower limit of $\sim 10^4\ M_\odot$ to their total dust mass as determined from IRAS observations (Bregman et al. 1998) or measured from optical absorption line measurements (Goudfrooij et al. 1994; Van Dokkum & Franx 1995; Ferrari et al. 1999). At 20 Mpc, a galaxy with a dust mass of $\sim 10^4\ M_\odot$ would have a flux density at 250 μm of 11 mJy. We estimate that with the adopted integration times we should detect an elliptical with $\sim 10^4\ M_\odot$ of dust at the 3σ level.

Integration times for spirals have been chosen so that we should be able to detect dust outside the optical radius,[28] for which there is evidence from ISO observations (Alton et al. 1998; Davies et al. 1999). By combining ISOPHOT (Alton et al. 1998) and SCUBA (Vlahakis et al. 2005) observations of extended sources with the spectral energy distribution of normal galaxies of different type (Boselli et al. 2003a), and assuming a standard gas-to-dust ratio of ∼100 with the extragalactic calibration for the dust-emissivity coefficient (James et al. 2002), we estimate that the dust associated with the extended HI disk would have a flux density of ∼14 mJy beam^{-1} at 250 μm for HI column densities of $\sim 10^{20}$ atoms cm^{-2}. In normal galaxies such gas column densities are generally reached well outside the stellar disk, at ∼1.5 optical radii (Cayatte et al. 1994; Broelis & Van Woerden 1994). Because of metallicity gradients, however, the gas-to-dust ratio is expected to increase in the outer disks, as observed in M31 by Cuillandre et al. (2001). We would therefore expect to observe lower far-IR flux densities. With 12 minutes of integration time (3 scan-maps) we will get to an instrumental noise of 6.9 mJy beam^{-1}, when the expected emission is 14 mJy beam^{-1}; this sensitivity will allow us to detect the dust emission in the outer disk by integrating flux densities along elliptical annuli with a sensitivity of ∼30 better than that of previous observations (Alton et al. 1998).

All galaxies outside the Virgo cluster will be observed in scan-map mode (30″ s^{-1}). For each galaxy, the size of the scan-map has been chosen based on the optical size of the galaxy. For late-type galaxies, the observing mode has been chosen so that our images will cover the galaxy at least out to $1.5 \times D_{25}$ (where D_{25} is the 25 mag arcsec^{-2} isophotal diameter) i.e. out to the approximate HI radius. For spirals we will make three pairs of cross-linked observations, which will reach a 1σ sensitivity in instrumental noise of 6.9, 4.6, and 6.9 mJy beam^{-1} at 250, 350, and 500 μm, respectively as determined during the science verification phase. These values are comparable to the noise from the confusion of faint unrelated sources (4, 5, and 6 mJy beam^{-1} in the three bands). Elliptical galaxies are likely to be weaker and thus need longer integration times, we have compromised by only requiring the image to contain the galaxy out to D_{25}. For ellipticals and S0s we will make eight pairs of cross-linked observations reaching a 1σ sensitivity in instrumental noise of 4.2, 2.8, and 4.2 mJy beam^{-1} at 250,

[27] For bright galaxies, we intend those included in major catalogs such as NGC, UGC, IC, or CGCG.

[28] Defined as the B-band isophotal radius at 25 mag arcsec^{-1}

TABLE 1

THE HERSCHEL REFERENCE SAMPLE

HRS (1)	CGCG (2)	VCC (3)	UGC (4)	NGC (5)	IC (6)	R.A. (J2000) (h m s) (7)	Decl. (° ′ ″) (8)	Type (9)	K_{Stot} (mag) (10)	D 25 (′) (11)	Velocity (km s^{-1}) (12)	Member (13)	Group (14)	A_B (mag) (15)	Other name (16)
1	123035	-	-	-	-	101739.66	224835.9	Pec	11.59	1.00	1175	Leo Cl.		0.13	
2	124004	-	5588	-	-	102057.13	252153.4	S?	11.03	0.52	1291	Leo Cl.		0.10	
3	94026	-	5617	3226	-	102327.01	195354.7	E2:pec;LINER;Sy3	8.57	3.16	1169	Leo Cl.	CP	0.10	KPG234A, ARP94
4	94028	-	5620	3227	-	102330.58	195154.2	SAB(s)pec;Sy1.5	7.64	5.37	1148	Leo Cl.	CP	0.10	KPG234B, ARP94
5	94052	-	-	-	610	102628.37	201341.5	Sc	9.94	1.86	1170	Leo Cl.		0.09	
6	154016	-	5662	3245A	-	102701.16	283821.9	SB(s)b	11.83	3.31	1322	Leo Cl.	CP	0.12	NGC 3245A
7	154017	-	5663	3245	-	102718.39	283026.6	SA(r)0:?;HII;LINER	7.86	3.24	1314	Leo Cl.	CP	0.11	
8	154020	-	5685	3254	-	102919.92	292929.2	SA(s)bc;Sy2	8.80	5.01	1356	Leo Cl.		0.09	
9	154026	-	5731	3277	-	103255.45	283042.2	SA(r)ab;HII	8.93	1.95	1415	Leo Cl.		0.11	
10	183028	-	5738	-	-	103429.82	351524.4	S?	11.31	0.91	1516	Leo Cl.		0.12	
11	124038	-	5742	3287	-	103447.31	213854.0	SB(s)d	9.78	2.09	1325	Leo Cl.		0.10	
12	124041	-	-	-	-	103542.07	260733.7	cI	11.98	0.59	1392	Leo Cl.		0.10	
13	183030	-	5753	3294	-	103616.25	371928.9	SA(s)c	8.38	3.55	1573	Leo Cl.		0.08	
14	124045	-	5767	3301	-	103656.04	215255.7	(R’)SB(rs)0/a	8.52	3.55	1341	Leo Cl.		0.10	
15	65087	-	5826	3338	-	104207.54	134449.2	SA(s)c	8.13	5.89	1300	Leo Cl.	3	0.14	
16	94116	-	5842	3346	-	104338.91	145218.7	SB(rs)cd	9.59	2.69	1260	Leo Cl.		0.12	
17	95019	-	5887	3370	-	104704.05	171625.3	SA(s)c	9.43	3.16	1281	Leo Cl.		0.13	
18	155015	-	5906	3380	-	104812.17	283606.5	(R’)SBa?	9.92	1.70	1604	Leo Cl.		0.11	
19	184016	-	5909	3381	-	104824.82	344241.1	SB pec	10.32	2.04	1630	Leo Cl.		0.09	
20	184018	-	5931	3395	2613	104950.11	325858.3	SAB(rs)cd pec:	9.95	2.09	1617	Leo Cl.	CP	0.11	KPG249A, ARP270
21	155028	-	5958	-	-	105115.81	275054.9	Sbc	11.56	1.45	1182	Leo Cl.	3	0.11	
22	155029	-	5959	3414	-	105116.23	275830.0	S0 pec;LINER	7.98	3.55	1414	Leo Cl.	3	0.11	
23	184028	-	5972	3424	-	105146.33	325402.7	SB(s)b:?;HII	9.04	2.82	1501	Leo Cl.	4	0.10	
24	184029	-	5982	3430	-	105211.41	325701.5	SAB(rs)c	8.90	3.98	1585	Leo Cl.	4	0.10	
25	125013	-	5995	3437	-	105235.75	225602.9	SAB(rs)c:	8.88	2.51	1277	Leo Cl.		0.08	
26	184031	-	5990	-	-	105238.34	342859.3	Sab	11.71	1.35	1569	Leo Cl.		0.08	
27	184034	-	6001	3442	-	105308.11	335437.3	Sa?	10.90	0.62	1734	Leo Cl.		0.08	
28	155035	-	6023	3451	-	105420.86	271422.9	Sd	10.23	1.70	1332	Leo Cl.		0.09	
29	95060	-	6026	3454	-	105429.45	172038.3	SB(s)c? sp;HII	10.67	2.09	1101	Leo Cl.	4	0.15	KPG257A
30	95062	-	6028	3455	-	105431.07	171704.7	(R’)SAB(rs)b	10.39	2.38	1105	Leo Cl.	4	0.14	KPG257B
31	267027	-	6024	3448	-	105439.24	541818.8	I0	9.47	5.62	1374	Ursa Maj. S S	CP	0.05	ARP205
32	95065	-	6030	3457	-	105448.63	173716.3	S?	9.64	0.91	1158	Leo Cl.	4	0.13	
33	95085	-	6077	3485	-	110002.38	145029.7	SB(r)b:	9.46	2.10	1432	Leo Cl.		0.09	
34	95097	-	6116	3501	-	110247.32	175922.2	Scd	9.41	3.89	1130	Leo Cl.	P	0.10	KPG263A
35	267037	-	6115	3499	-	110311.03	561318.2	I0	10.23	0.81	1522	Ursa Maj. S S		0.04	
36	155049	-	6118	3504	-	110311.21	275821.0	(R)SAB(s)ab;HII	8.27	2.69	1536	Leo Cl.	P	0.12	
37	155051	-	6128	3512	-	110402.98	280212.5	SAB(rs)c	9.65	1.62	1373	Leo Cl.	P	0.12	
38	38129	-	6167	3526	-	110656.63	071026.1	SAc pec sp	10.69	1.91	1419	Leo Cl.		0.14	
39	66115	-	6169	-	-	110703.35	120336.2	Sb:	11.13	1.86	1557	Leo Cl.		0.07	
40	67019	-	6209	3547	-	110955.94	104315.0	Sb:	10.44	1.91	1584	Leo Cl.	P	0.10	
41	96011	-	6267	3592	-	111427.25	171536.5	Sc? sp	10.78	1.78	1303	Leo Cl.		0.07	
42	96013	-	6277	3596	-	111506.21	144713.5	SAB(rs)c	8.70	4.06	1193	Leo Cl.		0.10	
43	96022	-	6299	3608	-	111658.96	180854.9	E2;LINER:	8.10	3.16	1108	Leo Cl.	5	0.09	KPG278B
44	96026	-	6320	-	-	111817.24	185049.0	S?	10.99	0.89	1121	Leo Cl.	CP	0.10	
45	291054	-	6330	3619	-	111921.60	574527.8	(R)SA(s)0+:	8.58	2.69	1544	Ursa Major Cl.	5	0.08	
46	96029	-	6343	3626	-	112003.80	182124.5	(R)SA(rs)0+	8.16	2.69	1494	Leo Cl.	CP	0.09	
47	156064	-	6352	3629	-	112031.82	265748.2	SA(s)cd:	10.50	2.29	1507	Leo Cl.		0.08	
48	268021	-	6360	3631	-	112102.85	531011.0	SA(s)c	7.99	5.01	1155	Ursa Major Cl.		0.07	
49	39130	-	6368	3640	-	112106.85	031405.4	E3	7.52	3.98	1251	Leo Cl.	4	0.19	
50	96037	-	6396	3655	-	112254.62	163524.5	SA(s)c:;HII	8.83	1.55	1500	Leo Cl.		0.11	
51	96038	-	6405	3659	-	112345.49	174906.8	SB(s)m?	10.28	2.09	1299	Leo Cl.		0.08	
52	268030	-	6406	3657	-	112355.57	525515.5	SAB(rs)c pec	10.29	1.45	1204	Ursa Major Cl.		0.07	
53	67071	-	6420	3666	-	112426.07	112032.0	SA(rs)c:	9.23	4.37	1060	Leo Cl.		0.14	
54	96045	-	6445	3681	-	112629.80	165147.5	SAB(r)bc; LINER	9.79	2.25	1244	Leo Cl.	4	0.11	
55	96047	-	6453	3684	-	112711.18	170149.0	SA(rs)bc;HII	9.28	2.89	1158	Leo Cl.	4	0.11	
56	291072	-	6458	3683	-	112731.85	565237.4	SB(s)c?;HII	8.67	1.86	1708	Ursa Major Cl.	3	0.07	
57	96049	-	6460	3686	-	112743.95	171326.8	SB(s)bc	8.49	3.19	1156	Leo Cl.	4	0.10	
58	96050	-	6464	3691	-	112809.41	165513.7	SBb?	10.51	1.35	1067	Leo Cl.	4	0.11	

TABLE 1 (*Continued*)

HRS (1)	CGCG (2)	VCC (3)	UGC (4)	NGC (5)	IC (6)	R.A. (J2000) (h m s) (7)	Decl. (° ′ ″) (8)	Type (9)	K_{Stot} (mag) (10)	D 25 (′) (11)	Velocity (km s^{-1}) (12)	Member (13)	Group (14)	A_B (mag) (15)	Other name (16)
59 ……	67084	-	6474	3692	-	112824.01	092427.5	Sb;LINER;HII	9.52	3.16	1717	Leo Cl.		0.14	
60 ……	268051	-	6547	3729	-	113349.34	530731.8	SB(r)a pec	8.73	2.82	991	Ursa Major Cl.	P	0.05	KPG209B
61 ……	292009	-	6575	-	-	113626.47	581129.0	Scd::HII	11.40	1.95	1217	Ursa Major Cl.	4	0.07	
62 ……	186012	-	6577	3755	-	113633.37	362437.2	SAB(rs)c pec	10.60	3.16	1571	Ursa Maj. S S		0.10	
63 ……	268063	-	6579	3756	-	113648.02	541736.8	SAB(rs)bc	8.78	4.17	1289	Ursa Major Cl.		0.05	
64 ……	292017	-	6629	3795	-	114006.84	583647.2	Sc;HII	10.64	2.14	1213	Ursa Major Cl.	3	0.06	
65 ……	292019	-	6640	3794	-	114053.42	561207.3	SAB(s)d	11.60	2.24	1383	Ursa Major Cl.		0.06	
66 ……	186024	-	6651	3813	-	114118.65	363248.3	SA(rs)b:	8.86	2.24	1468	Ursa Maj. S S		0.08	
67 ……	268076	-	6706	-	-	114414.83	550205.9	SB(s)m:	11.28	1.91	1436	Ursa Major Cl.		0.06	NGC 3846A
68 ……	186045	-	-	-	-	114625.96	345109.2	S?	11.44	0.32	1412	Ursa Maj. S S		0.09	MRK 429
69 ……	268088	-	6787	3898	-	114915.37	560503.7	SA(s)ab;LINE;HII	7.66	4.37	1171	Ursa Major Cl.		0.09	
70 ……	-	-	-	-	2969	115231.27	−035220.1	SB(r)bc?;HII	11.15	1.23	1617	Crater Cl.	3	0.12	
71 ……	292042	-	6860	3945	-	115313.73	604032.0	SB(rs)0+;LINER	7.53	5.25	1259	Ursa Major Cl.		0.12	
72 ……	-	-	-	3952	2972	115340.63	−035947.5	IBm: sp;HII	11.01	1.58	1577	Crater Cl.	3	0.11	
73 ……	269013	-	6870	3953	-	115348.92	521936.4	SB(r)bc;HII/LINER	7.05	6.92	1050	Ursa Major Cl.	P	0.13	
74 ……	269019	-	6918	3982	-	115628.10	550730.6	SAB(r)b:;HII;Sy2	8.85	2.34	1108	Ursa Major Cl.	4	0.06	
75 ……	269020	-	6919	-	-	115637.51	553759.5	Sdm:	11.56	1.45	1283	Ursa Major Cl.	4	0.06	
76 ……	269022	-	6923	-	-	115649.43	530937.3	Im:	11.32	2.00	1069	Ursa Major Cl.	4	0.12	
77 ……	13033	-	6993	4030	-	120023.64	−010600.0	SA(s)bc;HII	7.33	4.17	1458	Crater Cl.	P	0.11	
78 ……	98019	-	6995	4032	-	120032.82	200426.0	Im:	10.45	1.86	1269	Coma I Cl.		0.15	
79 ……	69024	-	7001	4019	755	120110.39	140616.2	SBb? sp	11.33	2.40	1508	Virgo Out.		0.14	
80 ……	69027	-	7002	4037	-	120123.67	132403.7	SB(rs)b:	10.11	2.51	932	Virgo Out.		0.12	
81 ……	13046	-	7021	4045	-	120242.26	015836.4	SAB(r)a;HII	8.75	3.00	2011	Virgo Out.		0.10	
82 ……	98037	-	-	-	-	120335.94	160320.0	Sab	11.19	0.60	931	Virgo Out.		0.13	KUG1201+163
83 ……	41031	-	7035	-	-	120340.14	023828.4	SB(r)a:;HII	11.82	1.10	1232	Crater Cl.		0.12	
84 ……	69036	-	7048	4067	-	120411.55	105115.8	SA(s)b:	9.90	1.20	2424	Virgo Out.		0.11	
85 ……	243044	-	7095	4100	-	120608.60	493456.3	(R’)SA(rs)bc;HII	8.03	5.37	1072	Ursa Major Cl.		0.10	
86 ……	41041	-	7111	4116	-	120736.82	024132.0	SB(rs)dm	10.27	3.80	1309	Virgo Out.	P	0.10	KPG322A
87 ……	69058	-	7117	4124	-	120809.64	102243.4	SA(r)0+	8.49	4.10	1652	Virgo Out.		0.12	
88 ……	41042	-	7116	4123	-	120811.11	025241.8	SB(r)c;Sbrst;HII	8.79	5.00	1326	Virgo Out.	P	0.09	KPG322B
89 ……	69088	66	7215	4178	-	121246.45	105157.5	SB(rs)dm;HII	9.58	5.35	369	Virgo N Cl.		0.12	
90 ……	13104	-	7214	4179	-	121252.11	011758.9	Sb(f)	7.92	3.80	1279	Virgo Out.		0.14	
91 ……	98108	92	7231	4192	-	121348.29	145401.2	SAB(s)ab;HII;Sy	6.89	9.78	−135	Virgo N Cl.		0.15	M 98
92 ……	69101	131	7255	-	3061	121504.44	140144.3	SBc? sp	10.64	2.60	2317	Virgo N Cl.		0.16	
93 ……	187029	-	7256	4203	-	121505.06	331150.4	SAB0-:;LINER;Sy3	7.41	3.39	1091	Coma I Cl.		0.05	
94 ……	69104	145	7260	4206	-	121516.81	130126.3	SA(s)bc:	9.39	5.10	702	Virgo N Cl.		0.14	
95 ……	69107	152	7268	4207	-	121530.50	093505.6	Scd	9.44	1.96	592	Virgo N Cl.		0.07	
96 ……	69110	157	7275	4212	-	121539.36	135405.4	SAc:;HII	8.38	3.60	−83	Virgo N Cl.		0.14	
97 ……	69112	167	7284	4216	-	121554.44	130857.8	SAB(s)b:;HII/LINER	6.52	9.12	140	Virgo N Cl.		0.14	
98 ……	69119	187	7291	4222	-	121622.52	131825.5	Sc	10.33	3.52	226	Virgo N Cl.		0.14	
99 ……	69123	213	7305	-	3094	121656.00	133731.0	S;BCD	11.25	0.93	−162	Virgo N Cl.		0.15	
100 …..	98130	226	7315	4237	-	121711.42	151926.3	SAB(rs)bc;HII	10.03	2.01	864	Virgo N Cl.		0.13	
101 …..	158060	-	7338	4251	-	121808.31	281031.1	SB0? sp	7.73	3.63	1014	Coma I Cl.		0.10	
102 …..	98144	307	7345	4254	-	121849.63	142459.4	SA(s)c	6.93	6.15	2405	Virgo N Cl.		0.17	M 99
103 …..	42015	341	7361	4260	-	121922.24	060555.2	SB(s)a	8.54	3.52	1935	Virgo B		0.10	
104 …..	99015	-	7366	-	-	121928.66	171349.4	Spiral	11.99	1.20	925	Virgo Out.		0.11	
105 …..	99014	355	7365	4262	-	121930.58	145239.8	SB(s)0-?	8.36	1.87	1369	Virgo A		0.15	
106 …..	42032	393	7385	4276	-	122007.50	074131.2	S(s)c II	10.69	2.10	2617	Virgo B		0.12	
107 …..	42033	404	7387	-	-	122017.35	041205.1	Sd(f)	10.74	1.89	1733	Virgo S Cl.		0.10	
108 …..	42037	434	-	4287	-	122048.49	053823.5	Sc(f)	11.02	1.76	2155	Virgo B		0.08	
109 …..	42038	449	7403	4289	-	122102.25	034319.7	SA(s)cd: sp	9.89	4.33	2541	Virgo S Cl.		0.09	
110 …..	70024	465	7407	4294	-	122117.79	113040.0	SB(s)cd	9.70	3.95	357	Virgo N Cl.	CP	0.15	KPG330B
111 …..	99024	483	7412	4298	-	122132.76	143622.2	SA(rs)c	8.47	3.60	1136	Virgo A	CP	0.15	KPG332A
112 …..	42044	492	7413	4300	-	122141.47	052305.4	Sa	9.53	2.16	2310	Virgo B		0.09	
113 …..	99027	497	7418	4302	-	122142.48	143553.9	Sc: sp	7.83	6.74	1150	Virgo A	CP	0.15	KPG332B
114 …..	42045	508	7420	4303	-	122154.90	042825.1	SAB(rs)bc;HII;Sy2	6.84	6.59	1568	Virgo S Cl.		0.10	M 61
115 …..	42047	517	7422	-	-	122201.30	050600.2	SBab(s)	10.79	1.41	1864	Virgo S Cl.		0.08	
116 …..	70031	522	7432	4305	-	122203.60	124427.3	SA(r)a	9.83	2.60	1888	Virgo A	CP	0.18	KPG333A
117 …..	70029	524	7431	4307	-	122205.63	090236.8	Sb	8.72	3.95	1035	Virgo B		0.10	
118 …..	42053	552	7439	-	-	122227.25	043358.7	SAB(s)cd	11.20	1.89	1296	Virgo S Cl.		0.10	

TABLE 1 (*Continued*)

HRS (1)	CGCG (2)	VCC (3)	UGC (4)	NGC (5)	IC (6)	R.A. (J2000) (h m s) (7)	Decl. (° ′ ″) (8)	Type (9)	K_{Stot} (mag) (10)	D 25 (′) (11)	Velocity (km s^{-1}) (12)	Member (13)	Group (14)	A_B (mag) (15)	Other name (16)
119	99029	559	7442	4312	-	122231.36	153216.5	SA(rs)ab: sp	8.79	5.10	153	Virgo A		0.12	
120	70034	570	7445	4313	-	122238.55	114803.4	SA(rs)ab: sp	8.47	5.10	1443	Virgo A		0.16	
121	70035	576	7447	4316	-	122242.24	091956.9	Sbc	9.25	2.48	1254	Virgo B		0.10	
122	99030	596	7450	4321	-	122254.90	154920.6	SAB(s)bc;LINER;HII	6.59	9.12	1575	Virgo A		0.11	M 100
123	42063	613	7451	4324	-	122306.18	051501.5	SA(r)0+	8.48	3.52	1670	Virgo S Cl.		0.10	
124	70039	630	7456	4330	-	122317.25	112204.7	Scd	9.51	5.86	1564	Virgo A		0.11	
125	42068	648	7461	4339	-	122334.94	060454.2	E0;Sy2	8.54	2.31	1298	Virgo B		0.11	
126	99036	654	7467	4340	-	122335.31	164319.9	SB(r)0+	8.32	3.60	930	Virgo A		0.11	
127	42070	656	7465	4343	-	122338.70	065714.7	SA(rs)b:	8.97	2.48	1014	Virgo B		0.09	
128	42072	667	7469	-	3259	122348.52	071112.6	SAB(s)dm?	11.06	1.89	1420	Virgo B		0.10	
129	99038	685	7473	4350	-	122357.81	164136.1	SA0;LINER	7.82	3.20	1241	Virgo A		0.12	
130	70045	692	7476	4351	-	122401.56	121218.1	SB(rs)ab pec:	10.24	2.92	2324	Virgo A		0.13	
131	42079	697	7474	-	3267	122405.53	070228.6	SA(s)cd	10.95	1.55	1231	Virgo B		0.10	
132	42080	699	7477	-	3268	122407.44	063626.9	Sm/Im	11.49	1.95	727	Virgo B		0.11	
133	158099	-	7483	4359	-	122411.06	313117.8	SB(rs)c? sp	10.81	3.60	1253	Coma I Cl.		0.11	
134	70048	713	7482	4356	-	122414.53	083208.9	Sc	9.69	3.20	1137	Virgo B		0.12	
135	42083	731	7488	4365	-	122428.23	071903.1	E3	6.64	8.73	1240	Virgo B		0.09	
136	42089	758	7492	4370	-	122454.93	072640.4	Sa	9.31	1.76	784	Virgo B		0.10	
137	70057	759	7493	4371	-	122455.43	114215.4	SB(r)0+	7.72	5.10	943	Virgo A		0.16	
138	70058	763	7494	4374	-	122503.78	125313.1	E1;LERG;LINER;Sy2	6.22	10.07	910	Virgo A		0.17	M 84
139	42093	787	7498	4376	-	122518.06	054428.3	Im	11.23	1.84	1136	Virgo B		0.10	
140	42092	785	7497	4378	-	122518.09	045530.2	(R)SA(s)a;Sy2	8.51	3.06	2557	Virgo S Cl.		0.07	
141	70061	792	7503	4380	-	122522.17	100100.5	SA(rs)b:?	8.33	3.52	971	Virgo B		0.10	
142	99044	801	7507	4383	-	122525.50	162812.0	Sa? pec;HII	9.49	2.60	1710	Virgo A		0.10	
143	42095	827	7513	-	-	122542.63	071300.1	SB(s)cd: sp	9.79	3.60	992	Virgo B		0.11	IC 3322A
144	70068	836	7520	4388	-	122546.82	123943.5	SA(s)b: sp;Sy2	8.00	5.10	2515	Virgo A		0.14	
145	70067	849	7519	4390	-	122550.67	102732.6	Sbc(s) II	10.33	2.18	1103	Virgo B		0.13	
146	42098	851	7518	-	3322	122554.12	073317.4	SAB(s)cd: sp	10.47	2.16	1195	Virgo B		0.12	
147	42099	859	7522	-	-	122558.30	032547.3	Sd(f)	10.18	2.92	1428	Virgo S Cl.		0.10	
148	99049	865	7526	4396	-	122558.80	154017.3	SAd: sp	10.34	3.36	−124	Virgo A		0.11	
149	70071	873	7528	4402	-	122607.56	130646.0	Sb	8.49	3.95	234	Virgo A		0.12	
150	70072	881	7532	4406	-	122611.74	125646.4	S0(3)/E3	6.10	11.37	−221	Virgo A		0.13	M 86
151	70076	912	7538	4413	-	122632.25	123639.5	(R')SB(rs)ab:	9.80	2.92	105	Virgo A		0.14	
152	42104	921	7536	4412	-	122636.10	035752.7	SB(r)b? pec;LINER	9.65	1.89	2289	Virgo S Cl.		0.08	
153	42105	938	7541	4416	-	122646.72	075508.4	SB(rs)cd:;Sbrst	10.97	2.18	1395	Virgo S Cl.		0.11	
154	70082	939	7546	-	-	122647.23	085304.6	SAB(s)cd	10.71	3.45	1271	Virgo B		0.13	NGC 4411B
155	70080	944	7542	4417	-	122650.62	093503.0	SB0: s	8.17	3.60	832	Virgo B		0.10	
156	99054	958	7551	4419	-	122656.43	150250.7	SB(s)a;LINER;HII	7.74	3.52	−273	Virgo A		0.14	
157	42106	957	7549	4420	-	122658.48	022939.7	SB(r)bc:	9.66	2.01	1695	Virgo S Cl.		0.08	
158	42107	971	7556	4423	-	122708.97	055248.6	Sdm:	11.05	3.06	1120	Virgo B		0.09	
159	70090	979	7561	4424	-	122711.59	092514.0	SB(s)a:;HII	9.09	4.33	438	Virgo B		0.09	
160	42111	1002	7566	4430	-	122726.41	061546.0	SB(rs)b:	9.35	3.02	1450	Virgo B	CP	0.08	KPG338A
161	70093	1003	7568	4429	-	122726.56	110627.1	SA(r)0+;LINER;HII	6.78	8.12	1130	Virgo A		0.14	
162	70098	1030	7575	4435	-	122740.49	130444.2	SB(s)0;LINER;HII	7.30	2.92	775	Virgo A		0.13	
163	70097	1043	7574	4438	-	122745.59	130031.8	SA(s)0/a pec:;LINER	7.27	8.12	70	Virgo A		0.12	
164	70099	1047	7581	4440	-	122753.57	121735.6	SB(rs)a	8.91	2.01	724	Virgo A		0.12	
165	42117	1048	7579	-	-	122755.39	054316.4	Sdm:	11.58	1.89	2252	Virgo B		0.09	
166	70100	1062	7583	4442	-	122803.89	094813.0	SB(s)0	7.29	5.05	517	Virgo B		0.10	
167	70104	1086	7587	4445	-	122815.94	092610.7	Sab: sp	9.83	3.20	328	Virgo B		0.11	
168	70108	1091	7590	-	-	122818.77	084346.1	Sbc	11.77	1.76	1119	Virgo B		0.09	
169	99063	-	7595	-	3391	122827.28	182455.1	Scd:	10.45	1.10	1701	Coma I Cl.		0.14	
170	99062	1110	7594	4450	-	122829.63	170505.8	SA(s)ab;LINER;Sy3	7.05	6.15	1954	Virgo A		0.12	
171	70111	1118	7600	4451	-	122840.55	091532.2	Sbc:	9.99	1.96	865	Virgo B		0.08	
172	99065	1126	7602	-	3392	122843.26	145958.2	SAb:	9.26	2.92	1687	Virgo A		0.16	
173	42124	1145	7609	4457	-	122859.01	033414.2	(R)SAB(s)0/a;LINER	7.78	2.92	884	Virgo S Cl.		0.09	
174	70116	1154	7614	4459	-	122900.03	135842.9	SA(r)0+;HII;LINER	7.15	3.36	1210	Virgo A		0.20	
175	70115	1158	7613	4461	-	122903.01	131101.5	SB(s)0+:	8.01	3.52	1919	Virgo A		0.10	
176	70121	1190	7622	4469	-	122928.03	084459.7	SB(s)0/a? sp	8.04	4.33	508	Virgo B		0.09	
177	42132	1205	7627	4470	-	122937.78	074927.1	Sa?;HII	10.12	1.84	2339	Virgo S Cl.		0.10	
178	42134	1226	7629	4472	-	122946.76	080001.7	E2/S0;Sy2;LINER	5.40	10.25	868	Virgo S Cl.		0.10	M 49

TABLE 1 (*Continued*)

HRS (1)	CGCG (2)	VCC (3)	UGC (4)	NGC (5)	IC (6)	R.A. (J2000) (h m s) (7)	Decl. (° ′ ″) (8)	Type (9)	K_{Stot} (mag) (10)	D 25 (′) (11)	Velocity (km s^{-1}) (12)	Member (13)	Group (14)	A_B (mag) (15)	Other name (16)
179	70125	1231	7631	4473	-	122948.87	132545.7	E5	7.16	4.04	2236	Virgo A		0.12	
180	70129	1253	7638	4477	-	123002.17	133811.2	SB(s)0:?;Sy2	7.35	3.60	1353	Virgo A		0.14	
181	70133	1279	7645	4478	-	123017.42	121942.8	E2	8.36	1.89	1370	Virgo A		0.11	
182	42139	1290	7647	4480	-	123026.78	041447.3	SAB(s)c	9.75	2.01	2438	Virgo S Cl.		0.10	
183	70139	1316	7654	4486	-	123049.42	122328.0	E+0−1 pec;NLRG;Sy	5.81	11.00	1292	Virgo A		0.10	M 87
184	70140	1326	7657	4491	-	123057.13	112900.8	SB(s)a:	9.88	1.89	497	Virgo A		0.18	
185	42141	1330	7656	4492	-	123059.74	080440.6	SA(s)a?	9.08	1.96	1777	Virgo S Cl.		0.11	
186	129005	-	7662	4494	-	123124.03	254629.9	E1−2;LINER	7.00	4.79	1310	Coma I Cl.		0.09	
187	42144	1375	7668	4505	-	123139.21	035622.1	SB(rs)m	9.56	4.76	1732	Virgo S Cl.		0.11	NGC 4496A, KPG343A
188	99075	1379	7669	4498	-	123139.57	165110.1	SAB(s)d	9.66	2.85	1505	Virgo A		0.13	
189	99077	1393	7676	-	797	123154.76	150726.2	SB(s)c II.5	10.80	1.69	2100	Virgo A		0.13	
190	99076	1401	7675	4501	-	123159.22	142513.5	SA(rs)b;HII;Sy2	6.27	7.23	2284	Virgo A		0.16	M 88
191	99078	1410	7677	4502	-	123203.35	164115.8	Scd:	11.90	1.48	1629	Virgo A		0.13	
192	70152	1419	7682	4506	-	123210.53	132510.6	Sa pec?	10.26	2.16	737	Virgo A		0.13	
193	70157	1450	7695	-	3476	123241.88	140301.8	IB(s)m:	10.91	2.60	−173	Virgo A		0.15	
194	14063	-	7694	4517	-	123245.59	000654.1	SA(s)cd: sp	7.33	11.00	1129	Virgo Out.	P	0.10	KPG344B
195	99087	1479	7703	4516	-	123307.56	143429.8	SB(rs)ab?	9.99	2.16	958	Virgo A		0.16	
196	70167	1508	7709	4519	-	123330.25	083917.1	SB(rs)d	9.56	3.60	1212	Virgo S Cl.		0.09	
197	70168	1516	7711	4522	-	123339.66	091029.5	SB(s)cd: sp	10.35	4.04	2330	Virgo S Cl.		0.09	
198	159016	-	7714	4525	-	123351.19	301639.1	Scd:	9.99	3.00	1174	Coma I Cl.		0.10	
199	99090	1532	7716	-	800	123356.66	152117.4	SB(rs)c pec?	10.58	1.96	2335	Virgo A		0.16	
200	42155	1535	7718	4526	-	123403.03	074156.9	SAB(s)0:	6.47	7.00	448	Virgo S Cl.		0.10	
201	42156	1540	7721	4527	-	123408.50	023913.7	SAB(s)bc;HII;LINER	6.93	5.86	1736	Virgo S Cl.		0.10	
202	70173	1549	7728	-	3510	123414.79	110417.7	S?	11.42	1.10	1357	Virgo A		0.13	
203	42158	1554	7726	4532	-	123419.33	062803.7	IBm;HII	9.48	2.60	2021	Virgo S Cl.		0.09	
204	42159	1555	7727	4535	-	123420.31	081151.9	SAB(s)c;HII	7.38	8.33	1962	Virgo S Cl.		0.08	
205	14068	1562	7732	4536	-	123427.13	021116.4	SAB(rs)bc;HII;Sbrst	7.52	7.23	1807	Virgo S Cl.		0.08	
206	42162	1575	7736	-	3521	123439.42	070936.0	SBm pec;BCD	11.01	2.00	597	Virgo S Cl.		0.10	
207	99093	1588	7742	4540	-	123450.87	153305.2	SAB(rs)cd;LINER;Sy1	9.24	2.60	1288	Virgo A		0.14	
208	99096	1615	7753	4548	-	123526.43	142946.8	SBb(rs);LINER;Sy	7.12	6.00	484	Virgo A		0.16	M 91
209	-	-	-	4546	-	123529.51	−034735.5	SB(s)0-:	7.39	3.31	1050	Virgo Out.		0.15	
210	70182	1619	7757	4550	-	123530.61	121315.4	SB0: sp;LINER	8.69	3.95	381	Virgo A		0.17	
211	70184	1632	7760	4552	-	123539.88	123321.7	E;LINER;HII;Sy2	6.73	7.23	322	Virgo A		0.18	M 89
212	99098	-	7768	4561	-	123608.14	191921.4	SB(rs)dm	10.63	1.51	1410	Coma I Cl.		0.11	KPG346A
213	129010	-	7772	4565	-	123620.78	255915.6	SA(s)b? sp;Sy3;Sy1.9	6.06	14.18	1233	Coma I Cl.	3	0.07	
214	70186	1664	7773	4564	-	123626.99	112621.5	E6	7.94	4.33	1165	Virgo A		0.15	
215	70189	1673	7777	4567	-	123632.71	111528.8	SA(rs)bc	8.30	2.92	2277	Virgo A	CP	0.14	KPG347A
216	70188	1676	7776	4568	-	123634.26	111420.0	SA(rs)bc	7.52	5.10	2255	Virgo A	CP	0.14	KPG347B
217	70192	1690	7786	4569	-	123649.80	130946.3	SAB(rs)ab;LINER;Sy	6.58	10.73	−216	Virgo A		0.20	M 90
218	42178	1692	7785	4570	-	123653.40	071448.0	S0(7)/E7	7.69	3.52	1730	Virgo S Cl.		0.10	
219	70195	1720	7793	4578	-	123730.55	093318.4	SA(r)0:	8.40	3.77	2284	Virgo E Cl.		0.09	
220	70197	1727	7796	4579	-	123743.52	114905.5	SAB(rs)b;LINER;Sy1.9	6.49	6.29	1520	Virgo A		0.18	M 58
221	42183	1730	7794	4580	-	123748.40	052206.4	SAB(rs)a pec	8.77	2.16	1032	Virgo S Cl.		0.10	
222	70199	1757	7803	4584	-	123817.89	130635.5	SAB(s)a?	10.46	1.96	1783	Virgo A		0.16	
223	42186	1758	7802	-	-	123820.82	075328.7	Sdm	11.76	1.89	1788	Virgo S Cl.		0.12	
224	42187	1760	7804	4586	-	123828.44	041908.8	SA(s)a: sp	8.47	4.33	792	Virgo S Cl.		0.16	
225	70202	1778	7817	-	3611	123904.14	132148.7	S?	11.42	1.76	2750	Virgo E Cl.		0.15	
226	42191	1780	7821	4591	-	123912.44	060044.3	Sb	10.24	1.96	2424	Virgo S Cl.		0.09	
227	14091	-	7819	4592	-	123918.74	0−3155.2	SA(s)dm:	10.22	5.75	1069	Virgo Out.		0.10	
228	-	-	-	-	-	123922.26	−053953.3	Pec	11.95	0.43	1199	Virgo Out.	CP	0.11	LCRSB123647.4−052325
229	70204	1809	7825	-	3631	123948.02	125826.1	S?	11.11	1.10	2839	Virgo E Cl.		0.17	
230	99106	1811	7826	4595	-	123951.91	151752.1	SAB(rs)b?	10.03	2.16	632	Virgo E Cl.		0.16	
231	70206	1813	7828	4596	-	123955.94	101033.9	SB(r)0+;LINER:	7.46	4.76	1834	Virgo E Cl.		0.10	
232	70213	1859	7839	4606	-	124057.56	115443.6	SB(s)a:	9.17	5.10	1645	Virgo E Cl.		0.14	
233	70216	1868	7843	4607	-	124112.41	115311.9	SBb? sp	9.58	3.95	2255	Virgo E Cl.		0.14	
234	70214	1869	7842	4608	-	124113.29	100920.9	SB(r)0	8.16	4.30	1864	Virgo E Cl.		0.07	
235	42205	1883	7850	4612	-	124132.76	071853.2	(R)SAB0	8.56	2.16	1875	Virgo S Cl.		0.11	
236	70223	1903	7858	4621	-	124202.32	113848.9	E5	6.75	7.67	444	Virgo E Cl.		0.14	M 59
237	42208	1923	7871	4630	-	124231.15	035737.3	IB(s)m?	9.89	2.31	742	Virgo S Cl.		0.13	
238	14109	-	7869	4629	-	124232.67	−012102.4	SAB(s)m pec	11.84	1.38	1116	Virgo Out.		0.16	

TABLE 1 (*Continued*)

HRS (1)	CGCG (2)	VCC (3)	UGC (4)	NGC (5)	IC (6)	R.A. (J2000) (h m s) (7)	Decl. (° ′ ″) (8)	Type (9)	K_{Stot} (mag) (10)	D 25 (′) (11)	Velocity (km s^{-1}) (12)	Member (13)	Group (14)	A_B (mag) (15)	Other name (16)
239	99112	1932	7875	4634	-	124240.96	141745.0	SBcd: sp	9.25	2.92	116	Virgo E Cl.	CP	0.12	KPG351B
240	70229	1938	7880	4638	-	124247.43	112632.9	S0-	8.21	2.01	1147	Virgo E Cl.		0.11	
241	43002	1939	7878	4636	-	124249.87	024116.0	E/S0/1;LINER;Sy3	6.42	9.63	1094	Virgo S Cl.		0.12	
242	70230	1943	7884	4639	-	124252.37	131526.9	SAB(rs)bc;Sy1.8	8.81	3.20	1048	Virgo E Cl.		0.11	
243	15008	-	7895	4643	-	124320.14	015842.1	SB(rs)0/a;LINER	7.41	3.00	1346	Virgo Out.		0.13	
244	71015	1972	7896	4647	-	124332.45	113457.4	SAB(rs)c	8.05	2.60	1422	Virgo E Cl.	CP	0.11	KPG353A
245	71016	1978	7898	4649	-	124340.01	113309.4	E2	5.74	5.10	1095	Virgo E Cl.	CP	0.11	M 60, KPG353B
246	100004	-	7901	4651	-	124342.63	162336.2	SA(rs)c;LINER	8.03	3.90	797	Virgo Out.		0.12	
247	71019	1987	7902	4654	-	124356.58	130736.0	SAB(rs)cd;HII	7.74	4.99	1039	Virgo E Cl.		0.11	
248	71023	2000	7914	4660	-	124431.97	111125.9	E5	8.21	1.89	1115	Virgo E Cl.		0.14	
249	71026	2006	7920	-	3718	124445.99	122105.2	S	11.91	2.60	844	Virgo E Cl.		0.13	
250	43018	-	7924	4665	-	124505.96	030320.5	SB(s)0/a	7.43	4.50	785	Virgo Out.		0.11	
251	15015	-	7926	4666	-	124508.59	−002742.8	SABc:;HII;LINER	7.06	4.57	1513	Virgo Out.	CP	0.11	
252	15016	-	7931	4668	-	124532.14	−003205.0	SB(s)d:;NLAGN	10.58	1.38	1619	Virgo Out.	CP	0.11	
253	15019	-	7951	4684	-	124717.52	−024338.6	SB(r)0+;HII	8.39	2.88	1490	Virgo Out.		0.12	
254	71043	2058	7965	4689	-	124745.56	134546.1	SA(rs)bc	7.96	5.86	1620	Virgo E Cl.		0.10	
255	43028	-	7961	4688	-	124746.46	042009.9	SB(s)cd	11.16	4.40	984	Virgo Out.		0.13	
256	15023	-	-	4691	-	124813.63	−031957.8	(R)SB(s)0/a pec;HII	8.54	2.82	1119	Virgo Out.		0.12	
257	71045	2070	7970	4698	-	124822.92	082914.3	SA(s)ab;Sy2	7.56	5.67	1008	Virgo E Cl.		0.11	
258	-	-	-	4697	-	124835.91	−054803.1	E6;AGN	6.37	7.24	1241	Virgo Out.		0.13	
259	43034	-	7975	4701	-	124911.56	032319.4	SA(s)cd	9.77	3.60	727	Virgo Out.		0.13	
260	100011	-	7980	4710	-	124938.96	150955.8	SA(r)0+? sp;HII	7.57	4.30	1129	Virgo Out.		0.13	
261	43040	-	7982	-	-	124950.19	025110.4	Sd(f)	10.17	3.39	1158	Virgo Out.		0.15	
262	43041	-	7985	4713	-	124957.87	051841.1	SAB(rs)d;LINER	9.75	3.20	652	Virgo Out.		0.12	
263	129027	-	7989	4725	-	125026.61	253002.7	SAB(r)ab pec;Sy2	6.17	9.66	1209	Coma I Cl.	3	0.05	
264	15027	-	7991	-	-	125038.96	012752.3	Sd(f)	11.61	1.70	1272	Virgo Out.		0.11	
265	-	-	-	4720	-	125042.78	−040921.0	Pec	10.77	0.65	1504	Virgo Out.		0.11	
266	-	-	-	4731	-	125101.09	−062335.0	SB(s)cd	9.79	6.61	1491	Virgo Out.		0.14	
267	129028	-	8005	4747	-	125145.96	254638.3	SBcd? pec sp	10.29	3.95	1179	Coma I Cl.	3	0.04	
268	71060	-	8007	4746	-	125155.37	120458.9	Sb: sp	9.50	2.20	1779	Virgo Out.		0.15	
269	71062	2092	8010	4754	-	125217.56	111849.2	SB(r)0-:	7.41	5.03	1377	Virgo E Cl.	P	0.14	KPG356A
270	15029	-	8009	4753	-	125222.11	−011158.9	I0	6.72	6.03	1239	Virgo Out.		0.15	
271	100015	-	8014	4758	-	125244.04	155055.9	Im:;HII	10.93	3.00	1240	Virgo Out.		0.11	
272	71065	2095	8016	4762	-	125256.05	111350.9	SB(r)0 sp;LINER	7.30	8.70	985	Virgo E Cl.	P	0.09	KPG356B
273	15031	-	8020	4771	-	125321.27	011609.0	SAd? sp;NLAGN	9.01	4.00	1119	Virgo Out.		0.09	
274	15032	-	8021	4772	-	125329.17	021006.0	SA(s)a;LINER;Sy3	8.36	2.90	1038	Virgo Out.		0.12	
275	-	-	-	4775	-	125345.70	−063719.8	SA(s)d	9.22	2.14	1566	Virgo Out.		0.15	
276	71068	-	8022	4779	-	125350.86	094235.7	SB(rs)bc;Sbrst	9.87	2.10	2832	Virgo Out.		0.09	
277	43060	-	-	4791	-	125443.97	080310.7	cI	11.35	1.20	2529	Virgo Out.		0.14	
278	71071	-	8032	-	-	125444.19	131414.2	S	10.39	2.75	1121	Virgo Out.		0.15	
279	15037	-	8041	-	-	125512.68	000700.0	SB(s)d	11.98	3.10	1321	Virgo Out.		0.10	
280	43066	-	8043	4799	-	125515.53	025347.9	S?	9.89	1.60	2802	Virgo Out.		0.15	
281	43068	-	8045	-	-	125523.62	075434.0	IBm:	11.82	0.91	2801	Virgo Out.		0.18	
282	43069	-	-	4803	-	125533.67	081425.8	Comp	10.71	0.50	2664	Virgo Out.		0.13	
283	43071	-	8054	4808	-	125548.94	041814.7	SA(s)cd:;HII	9.04	2.60	760	Virgo Out.		0.16	
284	-	-	-	-	3908	125640.62	−073346.1	SB(s)d?;HII	9.10	1.82	1296	Virgo Out.		0.15	
285	15049	-	8078	4845	-	125801.19	013433.0	SA(s)ab sp;HII	7.79	5.20	1097	Virgo Out.		0.09	
286	71092	-	8102	4866	-	125927.14	141015.8	SA(r)0+: sp;LINER	7.92	6.00	1986	Virgo Out.		0.12	
287	15055	-	8121	4904	-	130058.67	−000138.8	SB(s)cd;Sbrst	9.50	2.40	1174	Virgo Out.		0.11	
288	-	-	-	4941	-	130413.14	−053305.8	(R)SAB(r)ab:;Sy2	8.22	3.63	1114	Virgo Out.		0.16	
289	-	-	-	4981	-	130848.74	−064639.1	SAB(r)bc;LINER	8.49	2.75	1678	Virgo Out.		0.18	
290	189037	-	8271	5014	-	131131.16	361654.9	Sa? sp	10.11	1.70	1136	Canes Ven. Spur	3	0.03	
291	217031	-	8388	5103	-	132030.08	430502.3	Sab	9.49	1.45	1297	Canes Ven. Spur		0.08	
292	218010	-	8439	5145	-	132513.92	431602.2	S?;HII;Sbrst	9.33	2.00	1225	Canes Ven. Spur		0.05	
293	16069	-	8443	5147	-	132619.71	020602.7	SB(s)dm	9.73	1.91	1092	Virgo Out.		0.12	
294	246017	-	8593	-	902	133601.22	495739.0	Sb	10.42	2.19	1608	Canes Ven. Spur		0.05	
295	73054	-	8616	5248	-	133732.07	085306.2	(R)SB(rs)bc;Sy2;HII	7.25	1.79	1152	Virgo-Libra Cl.	P	0.11	
296	190041	-	8675	5273	-	134208.34	353915.2	SA(s)0;Sy1.9	8.67	2.75	1064	Canes Ven. Spur		0.04	KPG391A
297	246023	-	8711	5301	-	134624.61	460626.7	SA(s)bc: sp	9.11	4.17	1508	Canes Ven. Spur		0.07	
298	218047	-	8725	5303	-	134744.97	381816.4	Pec	10.23	0.91	1419	Canes Ven. Spur	CP	0.06	KPG397A

TABLE 1 (*Continued*)

HRS (1)	CGCG (2)	VCC (3)	UGC (4)	NGC (5)	IC (6)	R.A. (J2000) (h m s) (7)	Decl. (° ′ ″) (8)	Type (9)	K_{Stot} (mag) (10)	D 25 (′) (11)	Velocity (km s^{-1}) (12)	Member (13)	Group (14)	A_B (mag) (15)	Other name (16)
299	45108	-	8727	5300	-	134816.04	035703.1	SAB(r)c	9.50	3.89	1171	Virgo-Libra Cl.		0.10	
300	218058	-	8756	-	-	135035.89	423229.5	Sab	10.34	1.70	1354	Canes Ven. Spur		0.06	
301	17088	-	8790	5334	4338	135254.46	−010652.7	SB(rs)c:	9.94	4.17	1380	Virgo-Libra Cl.		0.20	
302	45137	-	8821	5348	-	135411.27	051338.8	SBbc: sp	10.87	3.55	1443	Virgo-Libra Cl.	5	0.12	
303	295024	-	8843	5372	-	135446.01	583959.4	S?	10.65	0.65	1717	Canes Ven-Came. Cl.		0.04	
304	46001	-	8831	5356	-	135458.46	052001.4	SABbc: sp;HII	9.64	3.09	1370	Virgo-Libra Cl.	5	0.11	
305	46003	-	8838	5360	958	135538.75	045906.2	I0	11.15	2.19	1171	Virgo-Libra Cl.	5	0.13	
306	46007	-	8847	5363	-	135607.21	051517.2	I0?	6.93	4.07	1136	Virgo-Libra Cl.	5	0.12	
307	46009	-	8853	5364	-	135612.00	050052.1	SA(rs)bc pec;HII	7.80	6.76	1242	Virgo-Libra Cl.	5	0.12	
308	46011	-	8857	-	-	135626.61	042348.0	Sb(f)	11.93	0.91	1091	Virgo-Libra Cl.		0.14	
309	272031	-	9036	5486	-	140724.97	550611.1	SA(s)m:	11.95	1.86	1383	Canes Ven-Came. Cl.	3	0.09	
310	47010	-	9172	5560	-	142005.42	035928.4	SB(s)b pec	9.98	3.72	1718	Virgo-Libra Cl.	3	0.13	ARP286
311	47012	-	9175	5566	-	142019.95	035600.9	SB(r)ab;LINER	7.39	6.61	1492	Virgo-Libra Cl.	3	0.13	ARP286
312	47020	-	9183	5576	-	142103.68	031615.6	E3	7.83	3.55	1482	Virgo-Libra Cl.	3	0.14	
313	47022	-	9187	5577	-	142113.11	032608.8	SA(rs)bc:	9.75	3.39	1490	Virgo-Libra Cl.	3	0.18	
314	19012	-	9215	-	-	142327.12	014334.7	SB(s)d	10.54	2.19	1389	Virgo-Libra Cl.		0.14	
315	220015	-	9242	-	-	142521.02	393222.5	Sc	11.73	5.01	1440	Canes Ven. Spur		0.05	
316	47063	-	9308	5638	-	142940.39	031400.2	E1	8.25	2.69	1845	Virgo-Libra Cl.	4	0.14	
317	47066	-	9311	-	1022	143001.85	034622.3	S?	11.70	1.10	1716	Virgo-Libra Cl.		0.15	
318	47070	-	9328	5645	-	143039.35	071630.3	SB(s)d	9.69	2.40	1370	Virgo-Libra Cl.		0.12	
319	75064	-	9353	5669	-	143243.88	095330.5	SAB(rs)cd	10.35	3.98	1368	Virgo-Libra Cl.		0.12	
320	47090	-	9363	5668	-	143324.34	042701.6	SA(s)d	11.71	3.31	1583	Virgo-Libra Cl.	P	0.16	
321	47123	-	9427	5692	-	143818.12	032437.2	S?	10.54	0.89	1581	Virgo-Libra Cl.		0.16	
322	47127	-	9436	5701	-	143911.06	052148.8	(R)SB(rs)0/a;LINER	8.14	4.27	1505	Virgo-Libra Cl.		0.16	
323	48004	-	9483	-	1048	144257.88	045324.5	S	9.55	2.24	1640	Virgo-Libra Cl.	CP	0.16	

TABLE 2
SPIRE PERFORMANCE

λ	250 μm	350 μm	500 μm
Ang. Res.	18.1″	25.2″	36.9″
Lin. Res.	1.7 kpc	2.4 kpc	3.6 kpc
Sensitivity	12 mJy beam^{-1}	8 mJy beam^{-1}	12 mJy beam^{-1}

NOTE.—1σ sensitivity (instrumental noise) for a standard map (one repeat = two crosslinked scans) as determined during the science verification phase (onboard observations). The linear resolution is at 20 Mpc.

350, and 500 μm, respectively, which in the latter two bands is below the noise expected from the confusion of faint sources.

Sixty square degrees centered on the Virgo cluster region will be covered by Herschel in parallel mode (i.e. using both SPIRE and PACS) as part of the Herschel Virgo Cluster Survey HeViCS.[29] Eighty-three HRS galaxies fall into this region. To avoid duplication, these galaxies will be observed only during the HeViCS survey. HeViCS will survey this region in fast-scan mode (60″ s^{-1}) using both SPIRE and PACS. The survey will make eight scans reaching a 1σ of instrumental noise of 4.5, 6.2, and 5.3 mJy beam^{-1} at 250, 350, and 500 μm, respectively, as determined using the Herschel Observation Planning Tool (HSpot ver. 4.2.0). This is not as deep as our observations of ellipticals and S0s outside Virgo, but the effect of confusion noise means that the decrease in effective sensitivity is really small. On the plus side, for the HRS galaxies in Virgo we will also have PACS images at 110 and 160 μm.

5. COMPLEMENTARY DATA

A number of key aims of our survey (see § 2) can only be achieved through the combination of Herschel observations with corollary data. UV to near-IR imaging is needed to determine the distribution and content of the different stellar populations, to quantify the intensity of the interstellar radiation field and to study the recent activity of star formation (UV and Hα). Optical spectroscopy is crucial to measure stellar and gas metallicities and to determine the presence of any nuclear activity. At the same time, the Balmer emission line can be used to measure the dust extinction within HII regions and are thus essential for quantifying the current level of star formation activity. HI and CO line data are necessary for determining the content and distribution of the gaseous component of the ISM, the principal feeder of star formation in galaxies. High resolution HI imaging can also be used to study the kinematical properties of the target galaxies. Mid-, far-IR and submillimeter data, combined with SPIRE data, will be used to study the physical properties of the different dust components (PAHs, very small grains, and large grains), and radio continuum data for measuring the thermal and synchrotron emission.

Given its definition, the HRS is easily accessible for ground-based and space facilities: the selected galaxies are in fact relatively bright ($m_B < 15$ mag) and extended (~2–3 arcmin). Listed in this section are the most important references for ancillary data.

5.1. UV, Optical, Near-IR, and Hα Imaging

Of the 323 galaxies in the HRS, 280 have been observed by the Galaxy Evolution Explorer (GALEX) in the two UV bands FUV ($\lambda_{\rm eff} = 1539$ Å, $\Delta\lambda = 442$ Å) and NUV ($\lambda_{\rm eff} = 2316$ Å, $\Delta\lambda = 1069$ Å). Observations have been taken as part of the Nearby Galaxy Survey (NGS; Gil de Paz et al. 2007), the Virgo cluster survey (Boselli et al. 2005), the All Imaging Survey (AIS) or as pointed observations in open time proposals. A GALEX legacy survey has been recently accepted to complete the UV observation of the HRS galaxies at a deepness of the Medium Imaging Survey (1500 s per field).

SDSS (DR7 release, Adelman-McCarthy et al. 2008) images in the *ugriz* filters are available for 313 objects. All galaxies have been observed in the JHK filters by 2MASS (Jarrett et al. 2003). Deep B, V, H, and K band images for all Virgo cluster galaxies and for some Coma I Cloud galaxies are available on the GOLDMine database[30] (Gavazzi et al. 2003). These have been taken with pointed observations during the near-infrared and optical extensive surveys of the Virgo cluster carried out by Boselli et al. (1997, 2000, 2003b) and Gavazzi et al. (2000b).

An Hα + [NII] imaging survey of the star-forming HRS galaxies found outside the Virgo cluster under way at the 2.1 m San Pedro Martir telescope is almost complete. Combined with images taken in the Virgo cluster region (Boselli & Gavazzi 2002, Boselli et al. 2002b; Gavazzi et al. 1998; 2002a; 2006) Hα + [NII] data are now available for 221 of the 258 late-type objects and 26 of the 65 early-types.

5.2. Integrated Spectroscopy

A low resolution ($R \sim 1000$), integrated spectroscopic survey in the wavelength range 3500–7200 Å is under way at the 1.93 m OHP telescope. In order to sample the spectral properties of the whole galaxy, and not just those of the nuclear regions (these last provided by the SDSS for 106 galaxies in the DR6), observations have been executed using the drifting technique described in Kennicutt (1992). Exposures are taken while constantly and uniformly drifting the spectrograph slit over the full extent of the galaxy. A resolution $R \sim 1000$ is mandatory for resolving [NII] from Hα and measuring the stellar underling Balmer absorption under Hβ.

Data for 64 Virgo cluster galaxies in the HRS have already been published in Gavazzi et al. (2004) along with a few other galaxies in Moustakas & Kennicutt (2006), Jansen et al. (2000) and Kennicutt (1992b). We have data from the literature or from

[29] At www.arcetri.astro.it/hevics.

[30] At http://goldmine.mib.infn.it/; Gavazzi et al. 2003

our own observations for $256/258$ of the late-types and $33/65$ of the early-types, making the whole sample complete at 89%. The remaining objects will be included in the future observing runs.

5.3. HI and CO Lines

Single-beam HI observations are available from a large variety of sources. Most of the galaxies have HI data in Springob et al. (2005) and Gavazzi et al. (2005), this last reference limited to the Virgo cluster region. Out of the 8 late-type galaxies, 249 have an HI measurements, as do $55/65$ of the early-types. All galaxies in the $0° < \text{decl.} < 30°$ range (80%) will be observed during the ALFALFA survey under way at the 305 m Arecibo radio telescope (Giovanelli et al. 2005). Data will be gathered with an homogeneous sensitivity (rms $= 2.5$ mJy) and spectral resolution ($5.5\ \text{km s}^{-1}$): at the average distance of the HRS the ALFALFA survey will detect all sources with $M_{HI} \geq 10^{7.5}\ M_{\odot}$. VLA and WSRT HI maps are available for 236 HRS galaxies, from the WHISP (van der Hulst 2002) and VIVA (Chung et al. 2009) survey, this last limited to the Virgo region, from VLA archives or from our own WSRT observations.

A $^{12}CO(1-0)$ line (2.6 mm, 115 GHz) survey of the HRS galaxies is under way at the 12 m Kitt Peak telescope. Fifty-eight spiral galaxies have been observed to date, with an average rms of 3 mK in T_R^* scale. Thanks to these new observations and to data in the literature, CO measurements are now available for $161/258$ late-type and $22/65$ early-type galaxies, with a detection rate of 83% and 55%, respectively. Data have been taken from different sources, mostly from the FCRAO survey of Young et al. (1995), or Kenney & Young (1988) and Boselli et al. (1995; 2002a) for the Virgo cluster region. We obtained time at the James Clerk Maxwell Telescope (JCMT) on the 345 GHz HARP array receiver to search for CO(3-2) emission from the central $3' \times 3'$ region (with $15''$ resolution) of a subsample of late-type galaxies with $K_{\text{Stot}} < 8.7$. As of the beginning of 2010 January, 42 of a total of 56 galaxies in the subsample have been observed to completion.

5.4. Mid-IR, Far-IR, and Submillimeter

Infrared data for the HRS galaxies are already available from different sources. $208/258$ late-type and $32/65$ of the early-type galaxies have been detected by IRAS at 60 and 100 μm, only 103 (Sa-Sd-Im-BCD) and 17 (E-S0-S0a) at 12 and 25 μm. Virgo galaxies have been observed with CAM (45), PHOT (26), and LWS (21) on ISO (Leech et al. 1999; Malhotra et al. 2001; Roussel et al. 2001; Boselli et al. 2002c, 2003b; Tuffs et al. 2002). Spitzer observations have been completed for 157 HRS galaxies with IRAC and 181 galaxies with MIPS. The data for all of these galaxies will eventually be available from the Spitzer archives. The pipeline-processed IRAC data are sufficient for science analysis, but MIPS data have been reprocessed using the MIPS Data Analysis Tools (Gordon et al. 2005) along with additional processing software.

All HRS galaxies have been observed during the recently completed AKARI all sky survey in the 9, 20, 70, 90, and 160 μm bands which covered ~95% of the whole sky with an angular resolution comparable to that of SPIRE (~$30''$ at 90 μm) and a sensitivity ~3 times better than IRAS. Pointed observations with AKARI and SCUBA are also available of a few ellipticals.

5.5. Radio Continuum Data

The HRS galaxies have been observed by the NVSS survey at 20 cm (1415 MHz) (Condon et al. 1998) with an angular resolution of $45''$ and a sensitivity of 2.5 mJy. Twenty-two of 65and $159/258$ of the early- and late-type galaxies, respectively, have been detected at 20 cm. The data of the FIRST survey, at $5''$ resolution, are also available (Becker et al. 1995). For a fraction of galaxies, data at 6.3 cm and 2.8 cm are also available from Niklas et al. (1995) and Vollmer et al. (2004).

5.6. X-ray data

X-ray data at 0.2–4 keV from the Einstein Observatory imaging instruments (IPC and HRI) are available for 31 early-type and 52 late-type galaxies from Fabbiano et al. (1992) and Shapley et al. (2001). Ten HRS galaxies have been detected by the ROSAT all sky survey (Voges et al. 1999), while *Chandra* observations of many of the early-type objects within the HRS are still under way (Gallo et al. 2008).

Table 3 gives the complete sample at different wavelengths, while Table 4 shows the availability of ancillary data for the HRS galaxies.

6. HRS DATA PROCESSING, DATA PRODUCTS, AND WEB SITE

The HRS galaxies are distributed widely across the sky, the survey will progress along with the Herschel mission, that is expected to last for three and a half years, with the first six months for commissioning, performance verification, science demonstration and the last three years for science. Data for each single observation will be proprietary for one year after it is taken. During this time, the data will be processed using the most up-to-date pipeline developed by the SPIRE-Instrument Control

TABLE 3
COMPLETENESS OF THE DATA SAMPLE

λ	E+S0+S0a	Sa-Sm-Im-BCD
K	100%	100%
HI	85% (40%)	97% (93%)
FIR (60 μm)	95% (62%)	89% (83%)
Radio cont. (20 cm)	100% (34%)	100% (62%)

NOTE.—Values in parentheses give the detection rate.

TABLE 4
Ancillary Data for the Herschel Reference Sample.

HRS	2MASS	SDSS	UV	Hα	IRAS	20 cm	HI	CO	Spec
1 …….	X	X	-	-	X	-	-	-	X
2 …….	X	X	X	-	X	X	X	-	X
3 …….	X	X	-	X	-	X	X	X	-
4 …….	X	X	-	X	X	X	X	X	X
5 …….	X	X	-	X	X	X	X	-	X
6 …….	X	X	X	-	-	-	X	-	-
7 …….	X	X	X	-	X	X	X	X	-
8 …….	X	X	X	X	X	-	X	X	X
9 …….	X	X	X	X	X	X	X	X	X
10 ……	X	X	-	-	X	X	X	-	X
11 ……	X	X	X	X	X	X	X	X	X
12 ……	X	X	X	-	X	-	X	-	X
13 ……	X	X	X	X	X	X	X	X	X
14 ……	X	X	X	-	X	X	X	-	-
15 ……	X	X	X	X	X	X	X	X	X
16 ……	X	X	X	X	X	-	X	X	X
17 ……	X	X	X	X	X	X	X	X	X
18 ……	X	X	X	X	X	X	X	-	X
19 ……	X	X	X	X	X	X	X	-	X
20 ……	X	X	X	X	-	X	X	X	X
21 ……	X	X	X	X	-	-	X	-	X
22 ……	X	X	X	X	-	X	X	-	-
23 ……	X	X	X	X	X	X	X	X	X
24 ……	X	X	X	X	X	X	X	X	X
25 ……	X	X	X	X	X	X	X	X	X
26 ……	X	X	X	-	X	-	X	-	X
27 ……	X	X	X	X	X	X	X	-	X
28 ……	X	X	X	X	X	X	X	-	X
29 ……	X	X	X	-	-	-	X	-	X
30 ……	X	X	X	-	-	X	X	-	X
31 ……	X	X	X	X	X	X	X	X	X
32 ……	X	X	X	X	-	-	X	X	X
33 ……	X	X	X	X	-	X	X	X	X
34 ……	X	X	X	X	-	X	X	X	X
35 ……	X	X	-	-	-	-	-	-	X
36 ……	X	X	X	X	X	X	X	X	X
37 ……	X	X	X	X	X	X	X	X	X
38 ……	X	X	-	X	X	X	X	X	X
39 ……	X	X	X	-	-	-	X	-	X
40 ……	X	X	X	X	-	X	X	-	X
41 ……	X	X	X	X	-	-	X	-	-
42 ……	X	X	-	X	-	X	X	X	X
43 ……	X	X	X	-	-	-	X	-	-
44 ……	X	X	X	-	-	X	X	-	X
45 ……	X	X	X	-	X	X	X	-	-
46 ……	X	X	-	-	-	X	X	-	-
47 ……	X	X	X	X	-	X	X	-	X
48 ……	X	X	X	X	X	X	X	X	X
49 ……	X	X	X	-	-	-	X	-	-
50 ……	X	X	X	X	X	X	X	X	X
51 ……	X	X	-	X	X	X	X	-	X
52 ……	X	X	X	-	X	X	X	-	X
53 ……	X	X	X	X	X	X	X	X	X
54 ……	X	X	X	X	X	-	X	X	X
55 ……	X	X	X	X	X	X	X	X	X
56 ……	X	X	X	X	X	X	X	X	X
57 ……	X	X	X	X	X	X	X	X	X
58 ……	X	X	X	X	X	X	X	-	X
59 ……	X	X	X	X	X	X	X	X	X

TABLE 4 (*Continued*)

HRS	2MASS	SDSS	UV	Hα	IRAS	20 cm	HI	CO	Spec
60	X	X	X	X	X	X	X	X	X
61	X	X	X	-	X	-	X	-	X
62	X	X	X	X	-	X	X	-	X
63	X	X	-	X	X	-	X	X	X
64	X	X	-	-	X	-	X	-	X
65	X	X	X	-	X	-	X	-	X
66	X	X	X	X	-	X	X	X	X
67	X	X	-	-	-	X	X	-	X
68	X	X	X	-	-	X	X	-	X
69	X	X	-	X	X	X	X	X	X
70	X	-	X	X	X	X	X	-	X
71	X	X	X	-	X	-	-	-	-
72	X	-	X	-	X	X	X	-	X
73	X	X	-	X	X	-	X	X	X
74	X	X	-	X	X	X	X	X	X
75	X	X	-	-	-	-	X	-	X
76	X	X	-	X	X	-	X	-	X
77	X	X	X	X	X	X	X	X	X
78	X	X	X	X	X	-	X	X	X
79	X	X	X	X	X	X	X	-	X
80	X	X	X	X	X	-	X	-	X
81	X	X	X	X	X	X	X	X	X
82	X	X	X	-	X	X	X	-	X
83	X	X	X	-	X	-	X	-	X
84	X	X	X	X	X	X	X	X	X
85	X	X	X	X	X	X	X	X	X
86	X	X	X	X	X	X	X	X	X
87	X	X	X	-	X	-	X	-	X
88	X	X	X	X	X	X	X	X	X
89	X	X	X	X	X	X	X	X	X
90	X	X	X	-	-	-	X	-	X
91	X	X	-	X	X	X	X	X	X
92	X	X	-	X	X	-	X	-	X
93	X	X	X	-	X	X	X	X	-
94	X	X	X	X	X	-	X	X	X
95	X	X	X	X	X	X	X	X	X
96	X	X	-	X	X	X	X	X	X
97	X	X	X	X	X	X	X	X	X
98	X	X	X	X	X	X	X	X	X
99	X	X	X	X	X	-	X	-	X
100	X	X	X	X	X	X	X	X	X
101	X	X	X	-	X	-	X	X	-
102	X	X	X	X	X	X	X	X	X
103	X	X	X	X	X	-	X	X	X
104	X	X	X	X	-	-	-	-	-
105	X	X	-	-	-	-	X	-	X
106	X	X	X	X	X	-	X	-	X
107	X	X	X	X	-	-	X	-	X
108	X	X	X	X	-	-	X	-	X
109	X	X	X	X	X	X	X	-	X
110	X	X	X	X	X	X	X	X	X
111	X	X	X	X	X	X	X	X	X
112	X	X	-	X	X	-	X	X	X
113	X	X	X	X	X	X	X	X	X
114	X	X	X	X	X	X	X	X	X
115	X	X	X	X	-	-	X	-	X
116	X	X	-	X	-	-	X	-	X
117	X	X	-	X	X	X	X	X	X
118	X	X	X	X	X	-	X	-	X
119	X	X	X	X	X	X	X	X	X

TABLE 4 (*Continued*)

HRS	2MASS	SDSS	UV	Hα	IRAS	20 cm	HI	CO	Spec
120	X	X	X	X	X	-	X	X	X
121	X	X	X	X	X	X	X	X	X
122	X	X	X	X	X	X	X	X	X
123	X	X	X	X	X	-	X	-	X
124	X	X	X	X	X	X	X	X	X
125	X	X	X	-	-	-	X	-	-
126	X	X	-	-	X	-	X	-	-
127	X	X	X	X	X	X	X	X	X
128	X	X	X	X	X	-	X	-	X
129	X	X	X	-	X	-	X	-	X
130	X	X	X	X	X	-	X	X	X
131	X	X	X	X	-	-	X	-	X
132	X	X	X	X	X	X	X	-	X
133	X	X	X	X	X	-	X	X	X
134	X	X	-	X	X	-	X	-	X
135	X	X	X	X	-	-	-	-	X
136	X	X	-	X	X	-	X	X	X
137	X	X	X	-	-	-	X	-	X
138	X	X	X	X	X	X	X	X	-
139	X	X	X	X	X	-	X	-	X
140	X	X	X	X	X	-	X	X	X
141	X	X	X	X	X	-	X	X	X
142	X	X	X	X	X	X	X	X	X
143	X	X	X	X	X	X	X	-	X
144	X	X	X	X	X	X	X	X	X
145	X	X	X	X	X	-	X	X	X
146	X	X	X	X	X	X	X	-	X
147	X	X	X	X	X	-	X	-	X
148	X	X	X	X	X	X	X	X	X
149	X	X	X	X	X	X	X	X	X
150	X	X	X	X	X	-	-	X	X
151	X	X	X	X	X	-	X	X	X
152	X	X	X	X	X	X	X	X	X
153	X	X	X	X	X	X	X	X	X
154	X	X	X	X	X	-	X	X	X
155	X	X	X	-	-	-	X	-	X
156	X	X	X	X	X	X	X	X	X
157	X	X	X	X	X	-	X	X	X
158	X	X	X	X	X	X	X	X	X
159	X	X	X	X	X	X	X	X	X
160	X	X	X	X	X	X	X	X	X
161	X	X	X	X	X	-	X	X	X
162	X	X	X	-	X	-	X	X	X
163	X	X	X	X	X	X	X	X	X
164	X	X	X	X	-	-	X	X	X
165	X	X	X	X	-	-	X	-	X
166	X	X	X	-	-	-	X	-	X
167	X	X	X	X	X	-	X	-	X
168	X	X	X	X	X	X	X	-	X
169	X	X	X	X	X	-	X	-	X
170	X	X	X	X	X	X	X	X	X
171	X	X	X	X	X	X	X	X	X
172	X	X	X	X	X	X	X	X	X
173	X	X	X	X	X	X	X	X	X
174	X	X	X	X	X	-	X	X	X
175	X	X	X	X	-	-	X	-	X
176	X	X	X	X	X	-	X	-	X
177	X	X	X	X	X	X	X	X	X
178	X	X	X	X	-	X	X	X	X
179	X	X	X	X	-	-	-	-	X

TABLE 4 (*Continued*)

HRS	2MASS	SDSS	UV	Hα	IRAS	20 cm	HI	CO	Spec
180	X	X	X	-	X	-	X	-	X
181	X	X	X	-	-	-	-	-	-
182	X	X	X	X	X	X	X	X	X
183	X	X	X	X	-	X	-	X	X
184	X	X	X	X	X	-	X	X	X
185	X	X	X	X	-	-	X	X	X
186	X	X	-	-	-	-	X	X	-
187	X	X	X	X	X	-	X	X	X
188	X	X	X	X	X	X	X	X	X
189	X	X	X	X	X	X	X	-	X
190	X	X	X	X	X	X	X	X	X
191	X	X	X	X	X	-	X	-	X
192	X	X	X	X	X	-	X	-	X
193	X	X	X	X	X	X	X	X	X
194	X	X	X	X	X	-	X	X	X
195	X	X	-	X	-	-	X	X	X
196	X	X	X	X	X	X	X	X	X
197	X	X	X	X	X	X	X	X	X
198	X	X	X	X	X	-	X	X	X
199	X	X	X	X	X	-	X	-	X
200	X	X	X	X	X	X	X	X	-
201	X	X	X	X	X	X	X	X	X
202	X	X	-	-	-	-	-	-	X
203	X	X	X	X	X	X	X	X	X
204	X	X	X	X	X	X	X	X	X
205	X	X	X	X	X	X	X	X	X
206	X	X	X	X	X	X	X	X	X
207	X	X	X	X	X	X	X	X	X
208	X	X	X	X	X	-	X	X	X
209	X	-	X	-	X	X	X	-	-
210	X	X	X	-	-	-	X	-	X
211	X	X	X	X	X	X	-	-	X
212	X	X	X	X	X	X	X	X	X
213	X	X	X	X	X	X	X	X	X
214	X	X	X	-	-	-	X	-	-
215	X	X	X	X	-	X	X	X	X
216	X	X	X	X	X	X	X	X	X
217	X	X	X	X	X	X	X	X	X
218	X	X	X	-	-	-	X	-	-
219	X	X	-	-	-	-	X	-	-
220	X	X	X	X	X	X	X	X	X
221	X	X	X	X	X	-	X	X	X
222	X	X	X	X	-	-	X	-	X
223	X	X	X	X	-	-	X	-	X
224	X	X	X	X	X	-	X	X	X
225	X	X	X	X	-	-	X	-	X
226	X	X	X	X	X	-	X	-	X
227	X	X	X	X	X	X	X	-	X
228	X	-	-	-	-	-	-	-	-
229	X	X	X	-	-	-	X	-	X
230	X	X	X	X	X	X	X	X	X
231	X	X	-	X	X	-	X	X	X
232	X	X	X	X	X	-	X	X	X
233	X	X	X	X	X	X	X	X	X
234	X	X	-	-	-	X	X	-	X
235	X	X	X	-	-	-	X	-	-
236	X	X	X	-	-	-	-	-	X
237	X	X	X	X	X	X	X	X	X
238	X	X	-	-	-	-	X	-	X
239	X	X	X	X	X	X	X	X	X

TABLE 4 (*Continued*)

HRS	2MASS	SDSS	UV	Hα	IRAS	20 cm	HI	CO	Spec
240	X	X	X	-	-	-	X	-	X
241	X	X	X	X	-	X	X	X	-
242	X	X	X	X	X	X	X	X	X
243	X	X	X	X	X	-	X	-	-
244	X	X	X	X	X	X	X	X	X
245	X	X	X	X	X	X	X	X	X
246	X	X	X	X	X	X	X	X	X
247	X	X	X	X	X	X	X	X	X
248	X	X	X	-	-	-	-	-	X
249	X	X	X	X	-	-	X	-	X
250	X	X	X	-	-	-	X	-	-
251	X	X	X	X	X	X	X	X	X
252	X	X	X	-	X	-	X	-	X
253	X	X	X	-	X	X	X	-	-
254	X	X	-	X	X	X	X	X	X
255	X	X	X	X	X	X	X	X	X
256	X	X	X	-	X	X	X	X	-
257	X	X	X	X	X	-	X	X	X
258	X	X	X	X	X	-	-	X	-
259	X	X	-	X	X	X	X	X	X
260	X	X	X	X	X	X	X	X	X
261	X	X	X	-	X	-	X	-	X
262	X	X	X	X	X	X	X	X	X
263	X	X	X	X	X	X	X	X	X
264	X	X	X	-	-	-	X	-	X
265	X	-	X	-	X	X	-	-	X
266	X	-	X	X	X	X	X	X	X
267	X	X	X	X	X	X	X	-	X
268	X	X	X	X	X	X	X	X	X
269	X	X	X	-	-	-	X	-	X
270	X	X	X	-	X	-	X	X	X
271	X	X	X	X	X	X	X	-	X
272	X	X	X	-	-	-	X	-	X
273	X	X	X	X	X	-	X	X	X
274	X	X	X	X	X	-	X	X	X
275	X	-	X	X	X	X	X	X	X
276	X	X	X	X	X	X	X	X	X
277	X	X	X	-	-	-	X	-	X
278	X	X	-	X	-	-	X	-	X
279	X	X	X	X	X	-	X	-	X
280	X	X	X	X	X	X	X	X	X
281	X	X	X	X	-	-	X	-	X
282	X	X	-	-	-	-	-	-	X
283	X	X	X	X	X	X	X	X	X
284	X	-	X	-	X	X	X	X	X
285	X	X	X	X	X	X	X	X	X
286	X	X	X	X	-	-	X	X	X
287	X	X	X	X	X	X	X	X	X
288	X	-	X	X	X	X	X	X	X
289	X	-	X	X	X	X	X	X	X
290	X	X	X	X	X	X	X	-	X
291	X	X	X	-	-	-	X	X	-
292	X	X	X	X	X	X	X	X	X
293	X	X	X	X	X	X	X	X	X
294	X	X	-	X	X	X	X	-	X
295	X	X	X	X	X	X	X	X	X
296	X	X	X	X	X	X	X	-	-
297	X	X	X	X	X	X	X	X	X
298	X	X	X	X	X	X	X	-	X
299	X	X	X	X	X	-	X	X	X

TABLE 4 (*Continued*)

HRS	2MASS	SDSS	UV	Hα	IRAS	20 cm	HI	CO	Spec
300	X	X	-	X	X	-	X	-	X
301	X	X	X	X	X	-	X	X	X
302	X	X	X	X	X	-	X	-	X
303	X	X	X	X	X	X	-	-	X
304	X	X	X	X	X	-	X	X	X
305	X	X	X	X	-	-	X	-	X
306	X	X	X	-	X	X	X	X	X
307	X	X	X	X	X	X	X	X	X
308	X	X	X	X	-	-	-	-	X
309	X	X	-	X	X	-	X	-	X
310	X	X	X	X	-	X	X	X	X
311	X	X	X	X	X	X	X	X	X
312	X	X	X	-	X	-	X	-	-
313	X	X	X	X	X	X	X	X	X
314	X	X	X	X	X	X	X	-	X
315	X	X	X	X	-	-	X	-	X
316	X	X	X	-	-	-	X	-	-
317	X	X	X	-	-	-	X	-	X
318	X	X	X	X	X	X	X	X	X
319	X	X	X	X	X	X	X	X	X
320	X	X	X	X	X	X	X	X	X
321	X	X	X	-	X	X	X	-	X
322	X	X	X	X	X	-	X	-	X
323	X	X	X	X	X	X	X	X	X

Centre since some members are also part of our consortium. This ensures we have access to the latest calibration files and bug fixes. Aside from the default data processing, the pipeline will also include new steps developed by the key-project teams (such as cosmic ray removal and baseline subtraction) for producing the most accurate representation of large-scale structures, such as the extended emission around galaxies. Additional postprocessing steps will be applied to prepare the data so that it can be easily used by the broader astronomical community. This will include reformatting the headers of the fits files so that they are easy to understand. Furthermore, the data will have been visually inspected so as to ensure that they suffer from no severe artefacts related to the observations or data reduction, and in cases where problems are identified, the data will be manually reprocessed to obtain the best results. After the proprietary time the team plans to make the reduced data available to the community through a dedicated web page. Herschel and ancillary data will be archived in an Information System at the Laboratoire d'Astrophysique de Marseille devel-opped under the SITools middleware interface (http://vds.cnes.fr/sitools/) with a Postgresql database. Images will be stored as fits files, and distributed in fits format while catalogs will be distributed in VO table and ASCII (cvs) format. The SPIRE data delivered by the team will be optimized for use by the wider astronomical community. Given the legacy nature of this project, we will also present through an interactive database all the ancillary data, X, UV, optical, near- and far-IR, submillimeter, and radio continuum fluxes and images, optical and line spectroscopy and derived parameters (structural parameters, metallicities, SFR…) with the aim of providing the community with a unique data set, a suitable reference for future studies.

7. THE STATISTICAL PROPERTIES OF THE HERSCHEL REFERENCE SAMPLE

In this section, we investigate how representative the HRS is of the galaxy population as a whole, thus unbiased versus cosmic variance. This is necessary since, as selected, the HRS is biased versus galaxies located in a high density environment (Virgo). One way to test this is to see whether the luminosity distributions at different wavelengths in the HRS are similar to the local galaxy luminosity functions at the corresponding frequencies.

Shown in Figure 3 is a comparison of the HRS luminosity distribution in the K band (histogram) to the K-band luminosity function of Cole et al. (2001) (dotted-dashed line; $\alpha = 0.96 \pm 0.05$, $M^*_K = -23.44 \pm 0.03$) and Kochanek et al. (2001) (solid line; $\alpha = 1.09 \pm 0.06$, $M^*_K = -23.39 \pm 0.05$), this last also considering separately early- (red dotted line; $\alpha = 0.92 \pm 0.10$, $M^*_K = -23.53 \pm 0.06$; color details can be seen in the online Figures) and late-type (blue dashed line; $\alpha = 0.87 \pm 0.09$, $M^*_K = -22.98 \pm 0.06$) galaxies. The Kochanek et al. (2001) values of the K-band luminosity function have

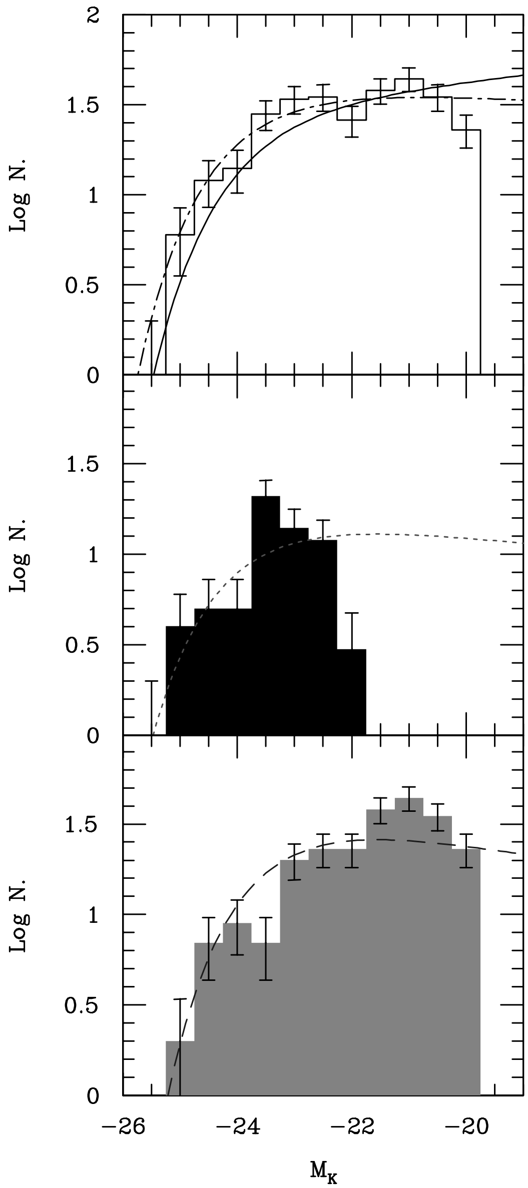

FIG. 3.—K band luminosity distribution of the HRS for all galaxies is compared to the 2MASS K band luminosity function of Kochanek et al. (2001) (*solid line*) and Cole et al. (2001) (*dotted-dashed line*), both in *upper panel*. The K band luminosity distributions of the E-S0-S0a (*center panel*) and Sa-Sd-Im-BCD (*lower panel*) galaxies in the HRS are compared to the Kochanek et al. (2001) K band luminosity function of early-type (*center panel, dotted line*) and late-type (*lower panel,dashed line*) galaxies. Poisson errors are also indicated. See the electronic edition of the *PASP* for a color version of this figure.

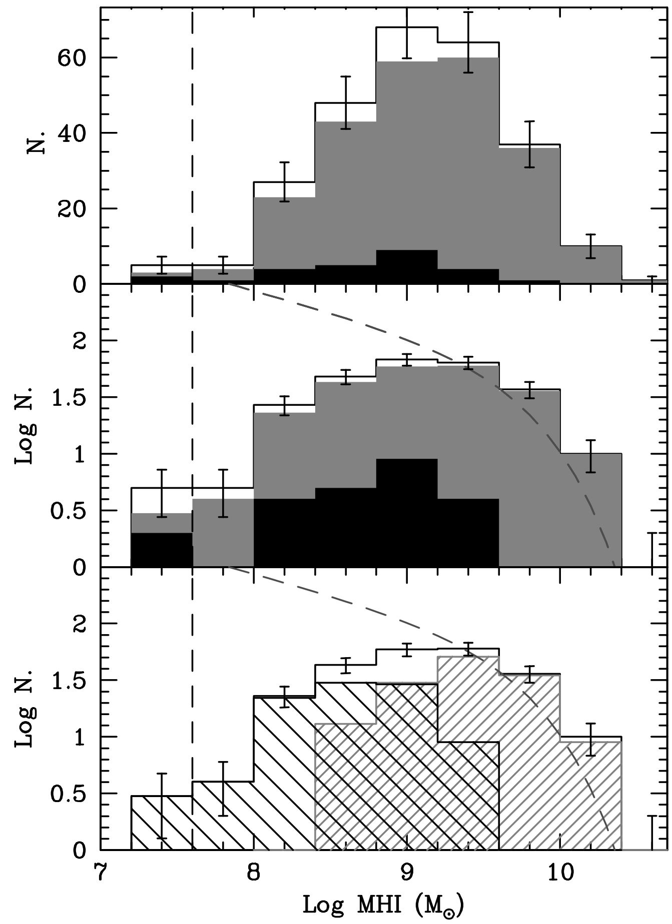

FIG. 4.—Atomic hydrogen mass distribution in linear (*upper panel*) and logarithmic (*middle panel*) scales for the HI-detected HRS galaxies (*empty histogram*). The *black* and *gray* histograms are for early-type (E-S0-S0a, 35% detected) and late-type (Sa-Sd-Im-BCD; 93% detected) galaxies, respectively. *Lower panel:* Atomic hydrogen mass distribution for late-type galaxies with a normal HI gas content (HI-deficiency <0.4; *tiny spaced hashed histogram*) and gas-poor galaxies (HI-deficiency ≥ 0.4; *large spaced hashed histogram*). *Curved dashed line* is the HI mass function determined by Zwaan et al. (2005); *vertical dashed line* indicates the detection limit of the ALFALFA survey (2.5 mJy) at the distance of 20 Mpc. See the electronic edition of the *PASP* for a color version of this figure.

been corrected to take into account the different assumed H_0, while the Cole et al. (2001) $M^*_{K\,S}$ Kron magnitudes have been converted into total magnitudes as in this work. The zero point of the plotted luminosity functions is determined assuming the same number of objects as HRS within the given magnitude limit. Figure 3 shows that, when considered from the perspective of the K band, the HRS is a good approximation to a volume-limited sample down to an absolute magnitude of $M_K \simeq -20$. This absolute magnitude limit is relatively high and explains why the HRS is underrepresented in Im and BCD galaxies (Fig. 2). The sample includes only the brightest ellipticals and lenticulars, whose K-band luminosity function ends at $M_K \sim -18$, while it does not include any quiescent dwarf system ($M_K \geq -20$).

Figure 4 shows the HI mass distribution of the HI-detected HRS early-type (black histogram) and late-type (gray histogram) galaxies compared to the HIPASS HI mass function determined by Zwaan et al. (2005) (dashed line, $\alpha = -1.37 \pm 0.03$, $M^*_{\rm HI} = 10^{9.8\pm0.03}\ M_\odot$ and ϕ^* arbitrarily normalized to match the data). The sample includes galaxies with HI masses ranging between $\sim 10^8$ and $10^{10}\ M_\odot$ but it is clearly under-representing galaxies with HI masses in the range $10^{7.5}$ $M_\odot \le M_{HI} \le 10^9$ $M_\odot$ which are easily detectable by an HI blind survey such as ALFALFA. The HIPASS HI mass function is dominated by gas rich, star-forming galaxies, while the HRS also includes quiescent, gas-poor early-types and HI-deficient cluster galaxies, as clearly observed in the Virgo cluster (Gavazzi et al. 2005; 2008) or in A1367 (Cortese et al. 2008b). The difference between the HIPASS mass function and the HRS HI mass distribution is due to (i) the fact that the HRS is K band selected and thus does not include gas rich, low-luminosity star-forming systems with HI masses in the range $10^{7.5} \le \mathrm{MHI} \le 10^{8.5}$ $M_\odot$ with K band magnitudes $12 \le K_{\mathrm{Stot}} \le 16$, and (ii) the presence of cluster HI-deficient late-type galaxies. Indeed, the HI mass distribution of galaxies with a normal HI gas content (HI-deficiency[31] <0.4) is more similar to the HIPASS mass function than the distribution of gas-poor objects (HI-deficiency ≥ 0.4). Most of the late-type HI-deficient objects (HI-deficiency ≥ 0.4) in the HRS are indeed located in the core of the Virgo cluster as shown in Figure 5. Galaxies in the outskirt of the Virgo cluster or in the surrounding clouds have a normal HI gas content (see Table 5) and can be generally considered as unperturbed objects (unless belonging to groups or pairs) in the study of the effects of the environment on the dust properties of galaxies. Indeed, despite the relatively poor statistics, the average HI-deficiency of late-type galaxies in the Coma I Cloud, Leo Cloud, Ursa Major Cloud and Southern Spur, Crater Cloud, Canes Venatici Spur, Canes Venatici–Camelopardalis Cloud, and Virgo–Libra Cloud is consistent with that of unperturbed galaxies in the reference sample of Haynes & Giovanelli (1984; HI-deficiency ≤ 0.3). The HI-deficiency of late-type galaxies in the different substructures of the Virgo cluster are generally consistent with those observed in a larger sample by Gavazzi et al. (1999a). The only exception is the Virgo E Cloud that we found to be dominated by HI-deficient objects. We notice, however, that the majority of the most HI-deficient galaxies (HI-deficiency >1.0) of the HRS belonging to this substructure are classified as early types in the VCC. The Coma I Cloud, previously thought to include gas-deficient objects (Garcia-Barreto et al. 1994; Gerin & Casoli 1994), is composed of galaxies with a normal gas content (Boselli & Gavazzi 2009). A detailed and complete study of the HI properties of late-type galaxies belonging to the other Clouds has not been done so far. A rather normal HI gas content of the spiral galaxies in the Ursa Major Cluster, a substructure of the Ursa Major Cloud, has been observed by Verheijen & Sancisi (2001).

[31] The HI-deficiency parameter is defined as as the logarithmic difference between the average HI mass of a reference sample of isolated galaxies of similar type and linear dimension and the HI mass actually observed in individual objects: $\mathrm{HI-def} = \log\ \mathrm{MHI_{ref}} - \log\ \mathrm{MHI_{obs}}$. According to Haynes & Giovanelli (1984), $\log \mathrm{MHI_{ref}} = a + b \times \log(\mathrm{diam})$, where a and b are weak functions of the Hubble type and diam is the linear diameter of the galaxy (see Gavazzi et al. 2005).

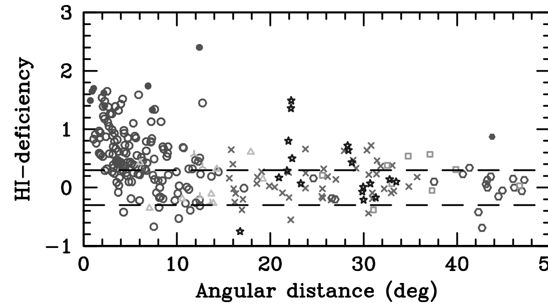

FIG. 5.—Variation of the HI-deficiency parameter as a function of the angular distance from the core of the Virgo cluster (M87). *Empty symbols* are for HI-detected galaxies, *filled symbols* for upper limits. See the electronic edition of the *PASP* for a color version of this figure with key to symbols.

Figure 6 shows the far-IR luminosity distribution of the HRS early-type (black histogram) and late-type (gray histogram) galaxies detected by IRAS at 60 μm compared the IRAS 60 μm luminosity function determined by Takeuchi et al. (2003) ($\alpha = 1.23 \pm 0.04$, $L^*_{60} = 8.85 \times 10^8\ L_\odot$, and ϕ^* in arbitrary units). The luminosity distribution of the HRS follows the luminosity function over 2 orders of magnitude. The low-luminosity cutoff is due to the detection limit of the IRAS survey. The lack of very luminous galaxies is because Luminous (LIRGs, $L_{60\ \mu\mathrm{m}} = 10^{11}\ L_\odot$) and Ultra Luminous (ULIRGs, $L_{60\ \mu\mathrm{m}} = 10^{12}\ L_\odot$) Infrared Galaxies are quite rare in the nearby universe and in particular inside rich clusters (Boselli & Gavazzi 2006).

TABLE 5
THE AVERAGE HI DEFICIENCY OF LATE-TYPE GALAXIES IN THE SUBSTRUCTURES

Substructure	Average	Standard Deviation	Number of Objects
Virgo A	0.91	±0.47	33
Virgo B	0.71	±0.46	25
Virgo N Cloud	0.39	±0.24	12
Virgo E Cloud	0.83	±0.53	12
Virgo S Cloud	0.47	±0.47	26
Virgo Outskirts	0.26	±0.60	38
Coma I Cloud	0.07	±0.35	8
Leo Cloud	0.11	±0.31	45
Ursa Major Cloud	0.05	±0.34	15
Ursa Major Southern Spur	−0.02	±0.20	4
Crater Cloud	0.13	±0.40	4
Canes Ven. Spur & Camelopardalis	0.19	±0.03	9
Virgo-Libra Cloud	0.31	±0.35	18

NOTE.—Upper limits are considered as detections.

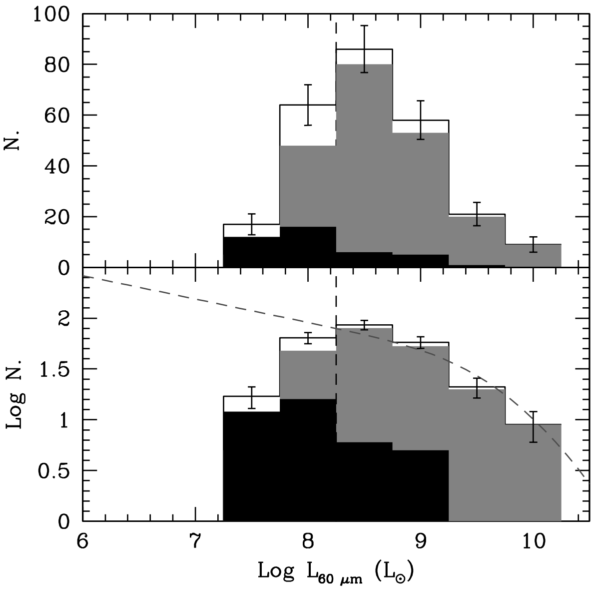

FIG. 6.—Infrared luminosity distribution in linear (*upper panel*) and logarithmic (*lower panel*) scales for the FIR (60 μm) detected HRS galaxies (*empty histogram*). The black and gray histograms are for early-type (E-S0-S0a) and late-type (Sa-Sd-Im-BCD) galaxies respectively. *Curved dashed line* is the IRAS 60 μm luminosity function determined by Takeuchi et al. (2003); *vertical dashed line* indicates the typical detection limit of IRAS (0.4 mJy) at the distance of 20 Mpc. See the electronic edition of the *PASP* for a color version of this figure.

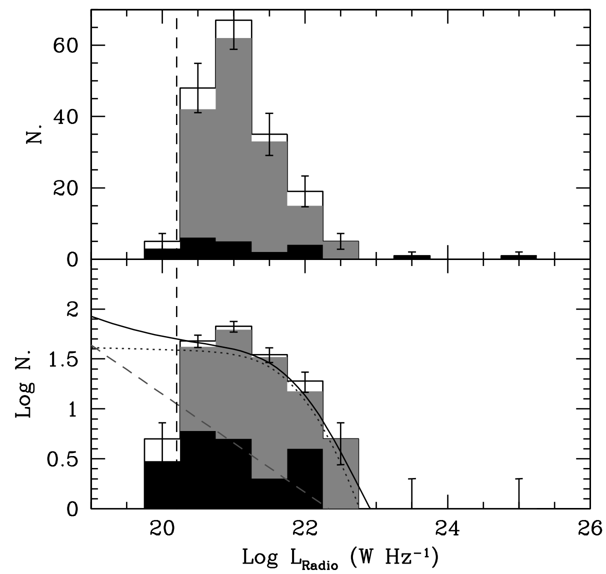

FIG. 7.—Radio continuum (1415 MHz) luminosity distribution in linear (*upper panel*) and logarithmic (*lower panel*) scales for the detected HRS galaxies (*empty histogram*). The black and gray histograms are for early-type (E-S0-S0a) and late-type (Sa-Sd-Im-BCD) galaxies, respectively, compared to the 2dF/NVSS luminosity function of Mauch & Sadler (2007, *solid line*). This radio luminosity function includes both the contribution of AGN (*dashed line*) and quiescent (*dotted line*) galaxies. *Vertical dashed line* indicates the typical detection limit of NVSS (2.5 mJy) at the distance of 20 Mpc. See the electronic edition of the *PASP* for a color version of this figure.

Figure 7 shows the radio continuum (1.4 GHz) luminosity distribution of the radio-detected HRS early-type (black histogram) and late-type (gray histogram) galaxies, as compared to the 2dF/NVSS luminosity function of Mauch & Sadler (2007) (solid line). This radio luminosity function includes the contribution from both AGN (dashed line) and quiescent (dotted line) galaxies. The radio luminosity distribution of the HRS is quite typical of normal, nearby galaxies ($10^{20} \leq L_{\rm Radio} \leq 10^{22}$ W $\rm Hz^{-1}$; Condon et al. 2002). The two brightest sources are the radio galaxies M87 (Virgo A, $L_{\rm Radio} = 10^{24.8}$ W $\rm Hz^{-1}$) and M84 ($L_{\rm Radio} = 10^{23.3}$ W $\rm Hz^{-1}$). The radio-continuum luminosity distribution as a whole agrees well with the field luminosity function, indicating that the contamination of cluster galaxies with an enhanced radio-continuum emission is minimal (Gavazzi & Boselli 1999c, 1999d).

In summary, since the K-band light traces stellar mass, the good agreement between the HRS luminosity distribution and K-band luminosity function implies that the HRS can be treated as a volume-limited sample down to a minimum stellar mass. Figure 6 shows that the HRS is also representative of a far-IR selected sample once the most active and rare in the local universe LIRG and ULIRG are excluded. The HRS matches also the distribution of a radio-continuum selected sample, although the statistic for the brightest radio galaxies is poor. However, Figure 4 shows that when viewed from the perspective of gas mass, the HRS is not a fair sample of the local universe. The presence of HI-deficient objects makes it ideal for studying the effects of the cluster environment on the dust properties of nearby galaxies.

We would like to thank the Herschel Project Scientist, G. Pilbratt; the SPIRE team; and all the people involved in the construction and the launch of Herschel. This research has made use of the NASA/IPAC Extragalactic Database (NED) which is operated by the Jet Propulsion Laboratory, California Institute of Technology, under contract with the National Aeronautics and Space Administration; and of the GOLD Mine database. A. B. wishes to thank S. Boissier for his help in the construction of the HRS database. We are grateful to the anonymous referee forinvaluable comments and suggestions which helped to improve the quality of the manuscript.

REFERENCES

Adelman-McCarthy, J., et al. 2008, ApJS, 175, 297
Alton, P., Trewhella, M., & Davies, J., et al. 1998, A&A, 335, 807
Alton, P., Trewhella, M., Davies, J., & Bianchi, S. 1999, A&A, 343, 51
Beker, R., White, R., & Helfand, D. 1995, ApJ, 450, 559

Bendo, G., Joseph, R., & Wells, M., et al. 2003, AJ, 125, 2361
Binggeli, B., Sandage, A., & Tammann, G. 1985, AJ, 90, 1681
Böhringer, H., Briel, U. G., Schwarz, R. A., Voges, W., Hartner, G., & Trumper, J. 1994, Nature, 368, 828
Boselli, A., & Gavazzi, G. 2002, A&A, 386, 124
———. 2006, PASP, 118, 517
———. 2009, A&A, 508, 201
Boselli, A., Casoli, F., & Lequeux, J. 1995, A&AS, 110, 521
Boselli, A., Tuffs, R., Gavazzi, G., Hippelein, H., & Pierini, D. 1997, A&A, 121, 507
Boselli, A., Gavazzi, G., Franzetti, P., Pierini, D., & Scodeggio, M. 2000, A&AS, 142, 73
Boselli, A., Gavazzi, G., Donas, J., & Scodeggio, M. 2001, AJ, 121, 753
Boselli, A., Lequeux, J., & Gavazzi, G. 2002a, A&A, 384, 33
Boselli, A., Iglesias-Páramo, J., Vilchez, J. M., & Gavazzi, G. 2002b, A&A, 386, 134
Boselli, A., Gavazzi, G., Lequeux, J., & Pierini, D. 2002c, A&A, 385, 454
Boselli, A., Gavazzi, G., & Sanvito, G. 2003a, A&A, 402, 37
Boselli, A., Sauvage, M., Lequeux, J., Donati, A., & Gavazzi, G. 2003b, A&A, 406, 867
Boselli, A., Lequeux, J., & Gavazzi, G. 2004, A&A, 428, 409
Boselli, A., Cortese, L., & Deharveng, J. M., et al. 2005a, ApJ, 629, L29
Bower, R. G., Lucey, J. R., & Ellis, R. S. 1992, MNRAS, 254, 601
Bregman, J., Snider, B., Grego, L., & Cox, C. 1998, ApJ, 499, 670
Bressan, A., Granato, G. L., & Silva, L. 1998, A&A, 332, 135
Bressan, A., Panuzzo, P., & Buson, L., et al. 2006, ApJ, 639, L55
Broelis, A. H., & Van Woerden, H. 1994, A&AS, 107, 129
Buat, V., & Xu, K. 1996, A&A, 306, 61
Buat, V., Boselli, A., Gavazzi, G., & Bonfanti, C. 2002, A&A, 383, 801
Calzetti, D. 2001, PASP, 113, 1449
Calzetti, D., Kennicutt, R., & Bianchi, L., et al. 2005, ApJ, 633, 871
Calzetti, D., Kennicutt, R., & Engelbracht, C., et al. 2007, ApJ, 666, 870
Catinella, B., Giovanelli, R., & Haynes, M. 2006, ApJ, 640, 751
Cayatte, V., Kotanyi, C., Balkowski, C., & van Gorkom, J. 1994, AJ, 107, 1003
Cayatte, V., van Gorkom, J., Balkowski, C., & Kotanyi, C. 1990, AJ, 100, 604
Chanial, P., Flores, H., Guiderdoni, B., Elbaz, D., Hammer, F., & Vigroux, L. 2007, A&A, 462, 81
Chung, A., van Gorkom, J., Kenney, J., Crowl, H., & Vollmer, B. 2009, AJ, 138, 1741
Cole, S., Norberg, P., & Baugh, C., et al. 2001, MNRAS, 326, 255
Condon, J. J., Cotton, W. D., & Broderick, J. J. 2002, AJ, 124, 675
Condon, J. J., Cotton, W. D., Greisen, E. W., Yin, Q. F., Perley, R. A., Taylor, G. B., & Broderick, J. J. 1998, AJ, 115, 1693
Cortese, L., Boselli, A., & Buat, V., et al. 2006, ApJ, 637, 242
Cortese, L., Boselli, A., Franzetti, P., Decarli, R., Gavazzi, G., Boissier, S., & Buat, V. 2008a, MNRAS, 386, 1157
Cortese, L., Minchin, R., & Auld, R., et al. 2008b, MNRAS, 383, 1519
Cortese, L., & Hughes, T. 2009, MNRAS, 400, 1225
Cowie, L., Songaila, A., Hu, E., & Cohen, J. 1996, AJ, 112, 839
Cuillandre, J. C., Lequeux, J., Allen, R., Mellier, Y., & Bertin, E. 2001, ApJ, 554, 190
Dale, D., Bendo, G., & Engelbracht, C., et al. 2005, ApJ, 633, 857
Dale, D., Gil de Paz, A., & Gordon, K., et al. 2007, ApJ, 655, 863
Davies, J., Alton, P., Bianchi, S., & Trewhella, M. 1998, MNRAS, 300, 1006
Davies, J., Alton, P., Trewhella, M., Evans, R., & Bianchi, S. 1999, MNRAS, 304, 495
Désert, F.-X., Boulanger, F., & Puget, J.-L. 1990, A&A, 237, 215
Devereux, N., & Young, J. 1990, ApJ, 359, 42
Disney, M., Davies, J., & Phillipps, S. 1989, MNRAS, 239, 939
Djorgovski, S., & Davis, M. 1987, ApJ, 313, 59
Draine, B. 1978, ApJS, 36, 596
Draine, B., & Li, A. 2007, ApJ, 657, 810
Draine, B., Dale, D., & Bendo, G., et al. 2007, ApJ, 663, 866
Dressler, A., Lynden-Bell, D., Burstein, D., Davies, R., Faber, S., Terlevich, R., & Wegner, G. 1987, ApJ, 313, 42
Duley, W., & Williams, D. 1986, MNRAS, 223, 177
Dunne, L., & Eales, S. 2001, MNRAS, 327, 697
Dunne, L., Eales, S., Edmunds, M., Ivison, R., Alexander, P., & Clements, D. 2000, MNRAS, 315, 115
Dwek, E. 1986, ApJ, 302, 363
Dwek, E., Arendt, R., & Fixsen, D., et al. 1997, ApJ, 475, 565
Eales, S., Wynn-Williams, C., & Duncan, W. 1989, ApJ, 339, 859
Engelbracht, C., Kundurthy, P., & Gordon, K., et al. 2006, ApJ, 642, L127
Fabbiano, G., Kim, D., & Trinchieri, G. 1992, ApJS, 80, 531
Ferrarese, L., Côté, P., & Jordán, A., et al. 2006, ApJS, 164, 334
Ferrari, F., Pastoriza, M. G., Macchetto, F., & Caon, N. 1999, A&AS, 136, 269
Galliano, F., Madden, S., Jones, A., Wilson, C., Bernard, J-P., & Le Peintre, F. 2003, A&A, 407, 159
Galliano, F., Madden, S., Jones, A., Wilson, C., & Bernard, J-P. 2005, A&A, 434, 867
Galliano, F., Dwek, E., & Chanial, P. 2008, ApJ, 672, 214
Gallo, E., Treu, T., Jacob, J., Woo, J. H., Marshall, P., & Antonucci, R. 2008, ApJ, 680, 154
Garcia-Barreto, J., Dowens, D., & Huchtmeier, W. 1994, A&A, 288, 705
Gavazzi, G., Pierini, D., & Boselli, A. 1996, A&A, 312, 397
Gavazzi, G., Catinella, B., Carrasco, L., Boselli, A., & Contursi, A. 1998, AJ, 115, 1745
Gavazzi, G., Boselli, A., Scodeggio, M., Pierini, D., & Belsole, E. 1999a, MNRAS, 304, 595
Gavazzi, G., Carrasco, L., & Galli, R. 1999b, A&AS, 136, 227
Gavazzi, G., & Boselli, A. 1999c, A&A, 343, 86
———. 1999d, A&A, 343, 93
Gavazzi, G., Franzetti, P., Scodeggio, M., Boselli, A., & Pierini, D. 2000a, A&A, 361, 863
Gavazzi, G., Franzetti, P., Scodeggio, M., Boselli, A., Pierini, D., Baffa, C., Lisi, F., & Hunt, L. 2000b, A&AS, 142, 65
Gavazzi, G., Boselli, A., Pedotti, P., Gallazzi, A., & Carrasco, L. 2002a, A&A, 396, 449
Gavazzi, G., Bonfanti, C., Sanvito, G., Boselli, A., & Scodeggio, M. 2002b, ApJ, 576, 135
Gavazzi, G., Boselli, A., Donati, A., Franzetti, P., & Scodeggio, M. 2003, A&A, 400, 451
Gavazzi, G., Zaccardo, A., Sanvito, G., Boselli, A., & Bonfanti, C. 2004, A&A, 417, 499
Gavazzi, G., Boselli, A., van Driel, W., & O'Neil, K. 2005, A&A, 429, 439

Gavazzi, G., Boselli, A., Cortese, L., Arosio, I., Gallazzi, A., & Pedotti, P. 2006, A&A, 446, 839
Gavazzi, G., Giovanelli, R., & Haynes, M., et al. 2008, A&A, 482, 43
Gerin, M., & Casoli, F. 1994, A&A, 290, 49
Giovanelli, R., Haynes, M., & Kent, B., et al. 2005, AJ, 130, 25, 98
Gil de Paz, A., Boissier, S., & Madore, B., et al. 2007, ApJS, 173, 185
Gordon, K., Perez-Gonzalez, P., & Misselt, K., et al. 2004, ApJS, 154, 215
Gordon, K., Rieke, G. H., & Engelbracht, C. W., et al. 2005, PASP, 117, 831
Goudfrooij, P., Hansen, L., Jorgensen, H. E., & Norgaard-Nielsen, H. U. 1994, A&AS, 105, 341
Griffin, M., Abergel, A., Ade, P., André, P., Baluteau, J-P., Bock, J., Franceschini, A., & Gear, W., et al. 2007, Adv. Space Res., 40 (5), 612
———. 2006, Proc. SPIE, 6265, 7
Guélin, M., Zylka, R., & Mezger, P. G., et al. 1993, A&A, 279, L37
Guélin, M., Zylka, R., Mezger, P. G., Haslam, C. G. T., & Kreysa, E. 1995, A&A, 298, L29
James, A., Dunne, L., Eales, S., & Edmunds, M. 2002, MNRAS, 335, 753
Jansen, R., Fabricant, D., Franx, M., & Caldwell, N. 2000, ApJS, 126, 331
Jarrett, T., Chester, T., Cutri, R., Schneider, S., & Huchra, J. 2003, AJ, 125, 525
Haynes, M., & Giovanelli, R. 1984, AJ, 89, 758
Heavens, A., Panter, B., Jimenez, R., & Dunlop, J. 2004, Nature, 428, 625
Hirashita, H., Buat, V., & Inoue, A. 2003, A&A, 410, 83
Hollenbach, D., & Salpeter, E. 1971, ApJ, 163, 155
Hollenbach, D., & Tielens, A. 1997, ARA&A, 35, 179
Holmberg, E. 1958, Lund Medd. Astron. Obs. Ser. II, 136, 1
Hughes, T., Cortese, L. 2009, MNRAS, 396, L41
Kaneda, H., Onaka, T., Kitayama, T., Okada, Y., & Sakon, I. 2007, PASJ, 59, 107
Karachentsev, I., Lebedev, V., & Shcherbanovskij, A. 1972, Publ. Special Astrophys. Obs. USSR 7
Kauffmann, G., Heckman, T., & White, S., et al. 2003, MNRAS, 341, 54
Kenney, J., & Young, J. 1988, ApJS, 66, 261
Kennicutt, R. 1992a, ApJ, 388, 310
———. 1992b, ApJS, 79, 255
———. 1998, ARA&A, 36, 189
Kennicutt, R., Armus, L., & Bendo, G., et al. 2003, PASP, 115, 928
Kennicutt, R., Calzetti, D., & Walter, F., et al. 2007, ApJ, 671, 333
Kochanek, C., Pahre, M., Falco, E., Huchra, J., Mader, J., Jarrett, T., Chester, T., Cutri, R., & Schneider, S. 2001, ApJ, 560, 566
Leech, K., Völk, H., & Heinrichsen, I., et al. 1999, MNRAS, 310, 317
Leeuw, L., Hawarden, T., Matthews, H., Robson, I., & Eckart, A. 2002, ApJ, 565, L131
Leeuw, L., Davidson, J., Dowell, K., & Matthews, H. 2008, ApJ, 677, L249
Malhotra, S., Kaufman, M., & Hollenbach, D., et al. 2001, ApJ, 561, 766
Mauch, T., & Sadler, E. 2007, MNRAS, 375, 931
Meiksin, A. 2009, Rev. Mod. Phys., 81, 1405
Montier, L., & Giard, M. 2005, A&A, 439, 35
Morton, R., & Haynes, M. 1994, ARA&A, 32, 115
Moustakas, J., & Kennicutt, R. 2006, ApJS, 164, 81
Neininger, N., Guélin, M., Garcia-Burillo, S., Zylka, R., & Wielebinski, R. 1996, A&A, 310, 725
Niklas, S., Klein, U., & Wielebinski, R. 1995, A&A, 293, 56
Nilson, P. 1973, The Uppsala General Catalogue of Galaxies (Uppsala: Uppsala Univ. Press)
Nolthenius, R. 1993, ApJS, 85, 1
Oppenheimer, B., & Davé, R. 2008, MNRAS, 387, 577
Panuzzo, P., Vega, O., & Bressan, A., et al. 2007, ApJ, 656, 206
Perez-Gonzalez, P., Kennicutt, R., & Gordon, K., et al. 2006, ApJ, 648, 987
Prescott, M., Kennicutt, R., & Bendo, G., et al. 2007, ApJ, 668, 182
Rayan-Weber, E., Pettini, M., & Madau, P. 2006, MNRAS, 371, L78
Roussel, H., Vigroux, L., & Bosma, A., et al. 2001b, A&A, 369, 473
Sarazin, C. 1986, Rev. Mod. Phys., 58, 1
Schlegel, F., Finkbeiner, D., & Davis, M. 1998, ApJ, 500, 525
Scodeggio, M., Gavazzi, G., Franzetti, P., Boselli, A., Zibetti, S., & Pierini, D. 2002, A&A, 384, 812
Shapley, A., Fabbiano, G., & Eskridge, P. 2001, ApJS, 137, 139
Skrutskie, M., Cutri, R., & Stiening, R., et al. 2006, AJ, 131, 1163
Soifer, B., Neugebauer, G., & Houck, J. 1987, ARA&A, 25, 187
Springob, C., Haynes, M., Giovanelli, R., & Kent, B. 2005, ApJS, 160, 149
Stickel, M., Klaas, U., Lemke, D., & Mattila, D. 2002, A&A, 383, 367
Takeuchi, T., Yoshikawa, K., & Ishii, T. 2003, ApJ, 587, L89
Temi, P., Brighenti, F., & Mathews, W. 2007, ApJ, 660, 1215
Tielens, A., McKee, C., Seab, C., & Hollenbach, D. 1994, ApJ, 431, 321
Thilker, D., Boissier, S., & Bianchi, L., et al. 2007, ApJS, 173, 572
Thomas, H., Dunne, L., Clemens, M., Alexander, P., Eales, S., Green, D., & James, A. 2002, MNRAS, 331, 853
Tremonti, C., Heckman, T., & Kauffmann, G., et al. 2004, ApJ, 613, 898
Tuffs, R., Popescu, C., & Pierini, D., et al. 2002, ApJS, 139, 37
Tully, B., & Fisher, J. 1977, A&A, 54, 661
Tully, B., Mould, J., & Aaronson, M. 1982, ApJ, 257, 527
Tully, B. 1988, Nearby Galaxy Catalog (Cambridge: Cambridge Univ. Press)
van der Hulst, J. 2002, in ASP Conf. Proc. 276, Seeing Through the Dust: The Detection of HI and the Exploration of the ISM in Galaxies, ed. A. R., Taylor, T. L., Landecker, & A. G., Willis (San Francisco: ASP) 84
Van Dokkum, P. G., & Franx, M. 1995, ApJ, 110, 2027
Verheijen, M., Sancisi, R. 2001, A&A, 370, 765
Visvanathan, N., Sandage, A. 1977, ApJ, 216, 214
Vlahakis, C., Dunne, L., Eales, S. 2005, MNRAS, 364, 1253
Voges, W., Aschenbach, B., & Boller, T. 1999, A&A, 349, 389
Vollmer, B., Thierbach, M., Wielebinski, R. 2004, A&A, 418, 1
Ward-Thompson, D., André, P., Kirk, J. 2002, MNRAS, 329, 257
Waskett, T., Sibthorpe, B., Griffin, J., Chanial, P. F. 2007, MNRAS, 381, 1583
Whittet, D. 1992, in Dust in the galactic environment (Graduate Series in Astronomy; Bristol: IOP Publishing)
Witt, A., Gordon, K. 2000, ApJ, 528, 799
Xilouris, E., Madden, S., Galliano, F., Virgoux, L., Sauvage, M. 2004, A&A, 416, 41
Young, J., Xie, S., Tacconi, L., et al. 1995, ApJS, 98, 219

Young, L., Bendo, G., Lucero, D. 2008 in The Evolving ISM in the Milky Way and Nearby Galaxies, 4th Spitzer Science Center Conf. (Pasadena, December 2007
Zaritsky, D., Kennicutt, R., Huchra, J. 1994, ApJ, 420, 87
Zubko, V., Dwek, E., Arendt, R. 2004, ApJS, 152, 211
Zwaan, M., Meyer, M., Staveley-Smith, L., & Webster, R. 2005, MNRAS, 359, L30
Zwicky, F., Herzog, E., Karpowicz, M., Kowal, C., & Wild, P. 1961 – 1968, Catalogue of Galaxies and of Cluster of Galaxies (CGCG; Pasadena: Caltech)